

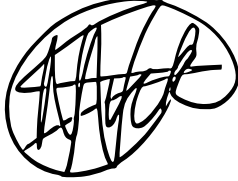
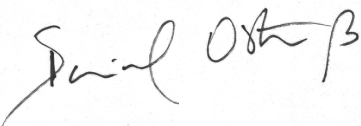
High mutational variance creates maladaptation around a phenotypic optimum

Nicholas O'Brien

Ortiz-Barrientos Laboratory

Word count: 8428 (Abstract: 243)

COVID-19 prevented a lot of contact with my supervisor over the year. As a result, some problems appeared after I had run my models which resulted in me changing my analysis methodology around 3.5 weeks before the deadline. Whilst this ultimately did not change my interpretation of results, it led to me having to discard about a month's worth of work. In addition, I had to shift the focus of my report from the effects of background selection to the effects of mutation rate on genetic variability due to another problem that I highlight in my methods.

Student name: Nicholas O'Brien	Student signature: 	Date: 11/11/20
Supervisor name: Daniel Ortiz-Barrientos	Supervisor signature: 	Date: 11/11/20

“The research carried out in the course of this investigation and the results presented in this report are, except where acknowledged, the original work of the author, and all research was conducted during the Honours program.”

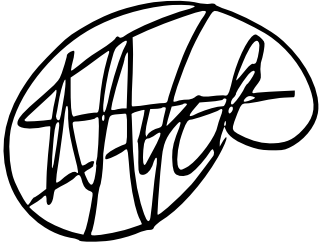
<p>Student name:</p> <p>Nicholas O'Brien</p>	<p>Student signature:</p> 	<p>Date:</p> <p>11/11/20</p>
--	---	------------------------------

TABLE OF CONTENTS

ABSTRACT	6
INTRODUCTION	7
METHODS	11
COMMON MODEL ELEMENTS	11
MODEL-SPECIFIC CHARACTERISTICS	13
MODEL PARAMETERIZATION	14
ANALYSIS	15
RESULTS	17
TRACKING POPULATION DYNAMICS OVER TIME	17
GENERAL PATTERNS OF ADAPTATION WITH CONTINUUM OF ALLELES MODELS	17
GENETIC ARCHITECTURE EFFECTS ON ADAPTATION WITH CONTINUUM OF ALLELES MODELS	18
ALLELIC EFFECT SIZE DISTRIBUTIONS WITH CONTINUUM OF ALLELES MODELS	20
DISCUSSION	22
ACKNOWLEDGMENTS	30
REFERENCES	31
TABLES	37
FIGURE LEGENDS	43
FIGURE 1	45
FIGURE 2	46
FIGURE 3	47
FIGURE 4	48
FIGURE 5	50
FIGURE 6	51
FIGURE 7	52
FIGURE 8	53
FIGURE 9	54

SUPPLEMENTARY MATERIAL	55
-------------------------------	-----------

FIGURE S1	55
FIGURE S2	56
FIGURE S3	57
FIGURE S4	59

Abstract

Despite the growing number of studies demonstrating the adaptive value of traits, natural populations are often maladapted. It is therefore likely that certain genetic characteristics impede adaptation, whereas others enable it. Building on the established quantitative genetics literature, I developed a novel methodology to simulate populations evolving through time under different evolutionary models: a Gaussian regime of allelic effects, representing high mutation rates and weak selection, and a House-of-Cards regime, characterized by low mutation rates and strong selection. I found that Gaussian populations became maladapted with increasing levels of mutational variance, whereas House-of-Cards populations were robust to changes in this variance. I discovered that the reason for this difference in robustness stemmed from how allelic effects were distributed at mutation-drift-selection balance in each model: distributions of allelic effects were unaffected by changes in mutational variance under House-of-Cards models, however, the distributions of allelic effects underlying Gaussian models were proportional to changes in mutational variance. Gaussian models were unable to 'regulate' their allelic effects, meaning high mutational variance was able to shift Gaussian populations away from the phenotypic optimum. This was not the case under House-of-Cards models. These dynamics lend credence to the evolution of mutation rates and the trade-off between adaptability and adaptedness, forming expectations as to which regime is most likely to be favoured in stable or dynamic environments. The methodology used here provides a framework for further exploration of quantitative genetics models through a population genetics lens, mediated by computational solutions.

Introduction

The ubiquity of adaptation in evolutionary studies is telling of the impact of natural selection in sculpting the shapes and forms of the natural world (DARWIN 1859). Although the ability of populations to adapt to new environments is wonderfully intuitive, natural populations are rarely perfectly adapted (BRADY *et al.* 2019). This is particularly apparent when adaptation relies on the evolution of polygenic traits, where many loci and alleles contribute to the correlation between fitness and a phenotype (FALCONER 1996). In such scenarios, a complex interaction between levels of genetic variability, genetic architecture, and evolutionary forces determines how populations approach and remain around a phenotypic optimum (Figure 1; GILBERT AND WHITLOCK 2017; WALSH AND LYNCH 2018). Maladaptation can thus be visualized as the stability of populations at some distance from a phenotypic optimum despite fitter phenotypes being available. Although maladaptation seems prevalent (BRADY *et al.* 2019), it is rarely discussed in light of quantitative genetic models of polygenic traits (NESSE 2005), making it difficult to reconcile views on adaptive walks towards a phenotypic optimum, and the maintenance of fitness around it.

Unravelling maladaptation in natural populations is nonetheless difficult, and studies rarely report it as it is perceived as a negative result (i.e. the absence of adaptation) (BRADY *et al.* 2019). A literature review by Estes and Arnold (2007) found that 64% of populations studied were at least one standard deviation away from the phenotypic optimum, consistent with the idea that adaptive landscapes limit the evolution of traits over time, and that maladaptation might be weak yet pervasive. Here, I investigate which evolutionary forces and genetic architectures maintain fitness variation around a phenotypic optimum, and discuss how my results shed light into trade-offs between adaptability (the ability to move towards a phenotypic optimum) and adaptedness (the ability to adhere to a phenotypic optimum over time) in nature. To answer these questions, I first describe the importance of additive genetic variance for adaptation.

Additive genetic variance, V_A , is the heritable component of a population's phenotypic variability (AGUIRRE *et al.* 2014). It is therefore an important predictor of a population's adaptability (LEWONTIN 1970; LYNCH AND LANDE 1998), where the more genetic variance a population maintains, the higher the chance of that population reaching a phenotypic optimal solution over time (LANDE AND SHANNON 1996). While

this might be true for populations responding to selection (FISHER 1930; BARTON AND CHARLESWORTH 1998), in stable environments genetic variance reduces population fitness by increasing the average distance of an individual from the phenotypic optimum (LANDE AND SHANNON 1996; BRADY *et al.* 2019). In other words, increasing V_A over time is generally favorable to track a moving phenotypic optimum (LASKY 2019), but hovering around a stable phenotypic optimum might require different levels of V_A . These levels of V_A result from the continued input of mutation, selection, and drift, and their effects on allelic frequencies (FALCONER 1996; WALSH AND LYNCH 2018).

Much of quantitative genetics theory is based on Fisher's infinitesimal model (1918), which provides an expectation for the inheritance of polygenic traits. This is summarized by the equation $P = G + E$, where P represents the phenotypic value, G is the genetic component of that value, which arises from the contribution of many alleles of small effects on the phenotype, and E represents the environmental error (FALCONER 1996; BARTON *et al.* 2017). Fisher's (1930) geometric model of adaptation is built upon the infinitesimal model. The geometric model assumes a stabilizing selection regime, where a phenotypic optimum lies at intermediate trait values (FISHER 1930; LANDE 1975). Peak fitness is usually assumed to lie at the maximum of a Gaussian or quadratic curve (WALSH AND LYNCH 2018). As populations move towards a phenotypic optimum and individuals become more similar, V_A is expected to decline (AGUIRRE *et al.* 2014; WALSH AND LYNCH 2018). As such, Fisher's models explain both the approach to the optimum, and the maintenance of the population around an optimum. However, these models are simplified versions of reality that have recently failed to explain the levels of genetic variability in natural populations (WALSH AND LYNCH 2018). As a consequence, a plethora of quantitative genetic models have been produced to address the origin and maintenance of genetic variance in nature (KIMURA 1965; LANDE 1975; TURELLI 1984).

The efficacy of stabilizing selection is partially dependent on genetic drift, which causes stochastic movement of phenotypes over time. Drift reduces V_A via random fixation or loss of alleles (LANDE 1976). The random nature of drift can therefore interfere with selection by preventing beneficial alleles from fixing (LYNCH *et al.* 2016). This process, referred to as the drift-barrier, is the displacement of weakly beneficial alleles by random fixations, which prevent populations from being perfectly adapted (LYNCH *et al.* 2016; WALSH AND LYNCH 2018). For adaptation to occur, the strength of

selection must overcome the strength of drift, either by increasing the population size or by increasing selection strength. As well as overcoming drift, populations must contend with the continuous influx of new mutations and genotypes to achieve adaptation.

Mutation rates in nature are usually low (less than 10^{-7} mutations per base pair per generation), because the vast majority of new mutations are deleterious (LYNCH *et al.* 2016; LABAR AND ADAMI 2017). High mutation rates carry a mutational load, where advantageous mutations that arise are likely to be linked to proportionally more deleterious mutations which kill the organism (LYNCH AND GABRIEL 1990; BRADY *et al.* 2019). This load prevents mutation rates from increasing (KIMURA 1967; MATIC 2019), particularly in regions of low recombination. In these regions, Hill-Robertson effects (HILL AND ROBERTSON 1966) are pronounced and recombination is necessary to separate beneficial alleles from their deleterious genetic background (OTTO 2009; ORTIZ-BARRIENTOS *et al.* 2016). Although mutation needs to be kept at bay, mutation creates new genetic variation, which is necessary for adaptation (LEWONTIN 1970). Thus, there must be a trade-off between limiting deleterious mutations and providing adequate V_A for adaptation, implying a direct connection between evolutionary forces during the origins and maintenance of adaptation/variation over long periods of time.

To study the maintenance of variability in populations hovering around a phenotypic optimum, I consider mutation-selection-drift models under the Continuum of Alleles (CoA) assumption, where many genes, each with many alleles, contribute to a trait (KIMURA 1965; LANDE 1975; FLEMING 1979). In these models, the distribution of additive effects impacts how much variation is predicted in populations hovering around such optimal phenotypes (HOULE *et al.* 2017; WALSH AND LYNCH 2018). For instance, although large-effect mutations can be beneficial early in the adaptive process, pushing populations closer to a phenotypic optimum (GILBERT AND WHITLOCK 2017), high mutational variance might reduce the fitness of populations hovering around a phenotypic optimum (Figure 1; CHARLESWORTH AND CHARLESWORTH 2010), as most large-effect mutations are expected to be deleterious post-adaptation (BARGHI *et al.* 2020).

Within CoA models, two regimes exist for the relative strengths of selection to mutation rate, giving rise to contrasting expected distributions of allelic effects (TURELLI 1984). Gaussian regimes describe weak selection and high mutation rates, resulting

in allelic distributions of small effects (KIMURA 1965; LANDE 1975; FLEMING 1979). House-of-Cards regimes assume strong selection and high mutation rates, with allelic distributions comprised of rarer, intermediate-sized effects (TURELLI 1984; HODGINS-DAVIS *et al.* 2015). The expectations of these models on mutational variability and adaptation are outlined in Figure 2. House-of-Cards models seem more common in nature, given empirical mutation rate and selection strength estimates (HODGINS-DAVIS *et al.* 2015; LYNCH *et al.* 2016; WALSH AND LYNCH 2018), although in species with low recombination rates, Gaussian regimes might be apt (LYNCH AND GABRIEL 1983; CHARLESWORTH 1993). Understanding the consequences of mutational variability on genetic variance during adaptation could reveal which environmental and genetic circumstances favor high mutation rates. However, the costs of pleiotropy on adaptation must also be considered.

Pleiotropy is often associated with the cost of complexity, where the number of traits an organism possesses is negatively correlated with its adaptability (ORR 2000). Pleiotropy reduces the efficiency of selection by restricting available variance (SZTEPANACZ AND BLOWS 2017). Mutational correlations can similarly constrain responses to selection (CHANTEPIE AND CHEVIN 2020). Together with additive effect variability and recombination, pleiotropic effects are likely to perturb equilibrium levels of V_A in populations at mutation-selection-drift balance. How these parameters affect a population's distance to a phenotypic optimum under Gaussian and House-of-Cards regimes remains a mystery, but recent advances in individual-based forward genetics modelling software has enabled the integration of quantitative models with population genetics (HALLER AND MESSER 2019), showing new promise in addressing these gaps in knowledge.

Here, I use novel computational experiments to simulate Gaussian and House-of-Cards models maintaining their position from a multi-trait phenotypic optimum over time. I explore the interaction of multiple evolutionary forces with varying genetic architectures to reveal the underlying distributions of alleles that maintain variability around a phenotypic optimum. Overall, I provide insights into how variance-covariance structures and distributions of alleles create genetic architectures that might enable the maintenance of adaptation in nature.

Methods

Using the forward-genetics modelling package SLiM 3.4 (HALLER AND MESSER 2019), I constructed two models to explore a portion of the multivariate parameter space that explains genetic variability in natural populations. These parameters included genome-wide recombination rate, the additive effect size variance, the rate of universal pleiotropy, mutational correlation between traits, and the selection strength multiplier (Table 1). The relative rate of non-quantitative trait locus (QTL), deleterious mutation compared to trait mutations was also varied across models. Due to its implementation, this parameter was confounded with mutation rate. This led to two explanations for effects on adaptation and variability: either the reduction in QTL mutation rate due to increasing deleterious mutation rate could cause observed differences, or the effect of the deleterious mutations on fitness could be attributed to the differences. Preliminary analyses indicated that the ratio of QTL mutations to deleterious mutations remained constant across increasing levels of this parameter (Figure S1). This suggests that a similar deleterious load was experienced across populations. Hence, the effects of increasing this parameter were attributable to changes in QTL mutation rate rather than the deleterious effects of non-QTL mutations. The highest QTL mutation rates were experienced by models with low rates of deleterious mutation and vice versa. Thus, models with a high mutation rate and low selection strength (deleterious mutation rate < 0.33 ; $\tau > 660$) approximated the Kimura-Fleming-Lande Gaussian model of allelic effects (KIMURA 1965; LANDE 1975; FLEMING 1979), while models with a low mutation rate and high selection strength approximated Turelli's (1984) House-of-Cards model. Among all parameter combinations, multiple conditions and assumptions were shared.

Common model elements

Both of my experimental models consisted of a SLiM model simulating a Wright-Fisher population of 8000 diploid individuals evolving over 100,000 generations. Populations were first subject to 50,000 generations of neutral burn-in to build standing variation to mutation-drift balance (Figure S2). Individuals were characterized by eight traits, controlled by 100 loci each. Each trait had an identical effect on fitness, similar to an exchangeable model of loci, but on traits (WALSH AND LYNCH 2018). This formed a 'mega-trait' with varying variance-covariance structures depending on pleiotropy rates. Each locus was assumed to have identical length, 1346 base pairs. This is

based on the average number of base pairs in eukaryotes (XU *et al.* 2006). Mutations were assumed to occur at an arbitrary position within the locus. This assumption is supported by a study by Thornton (2019), which found that within-locus differences in linkage had no average effect on either genetic variance or the mean trait value, indicating within-locus independence. Mutations were assumed to be completely additive in effect, contributing to traits in phenotypic units: an arbitrary unit denoting relative differences in phenotype. All loci were assumed to be on the same chromosome, with genetic distance being determined by the recombination rate parameter, r (Table 1). Both models had a genome-wide germline mutation rate of 8.045×10^{-6} per locus per generation, based on an average of five groups of eukaryotes (ASTON *et al.* 2017).

The effective population size, $N_e = 8000$, was chosen to compromise between computational performance and the effect of genetic drift on populations under stabilizing selection. This value results in weak genetic drift in comparison with the strength of selection (under strong selection pressures), and appropriate standing genetic variation following burn-in to allow for adaptation (LYNCH AND LANDE 1998). Mutational effects on trait values were sampled from a normal distribution,

$$N(0, \alpha),$$

where α is the additive effect size (Table 1). In the case of pleiotropy, a multivariate normal distribution was used for sampling effects for all eight traits,

$$N(0, \Sigma),$$

where Σ is a covariance matrix with diagonal values equal to α and non-diagonals pulled from a normal distribution:

$$N(m\alpha, 0.2m\alpha),$$

where m is the mutational correlation (Table 1).

Non-trait deleterious mutations had fitness effects sampled from a gamma distribution:

$$P(s \mid \varepsilon, \beta) = [\Gamma(\alpha)\beta^\varepsilon]^{-1} s^{\varepsilon-1} \exp\left(\frac{-s}{\beta}\right),$$

where $\varepsilon = 0.2$ and $\beta = -0.15$ (HALLER 2016). This describes a distribution of weak deleterious mutations on average.

All models were subject to 50,000 generations of neutral burn-in, where mutations accumulate until the population reaches mutation-drift equilibrium. This is tracked as heterozygosity through the simulation, where mutation-drift equilibrium occurs when:

$$\theta = 4N_e\mu \quad (1)$$

where μ represents the per-locus mutation rate per generation, and N_e is the effective population size (KIMURA AND CROW 1964). A population at equilibrium was assumed sufficiently burnt in. Trials (not shown) indicated that 50,000 generations of burn-in were sufficient for population sizes under 10,000 (Figure S2). Deleterious mutation/QTL mutation rate lowered θ , driving heterozygosity away from expectation in initial burn-in tests (not shown). However, an alternative equilibrium was reached, satisfying the requirements of burn-in regardless of the parameter. I collected trait variances, covariances, and trait means every 500 generations to track distances from the phenotypic optimum and trait variability over time. I collected the allelic effects of segregating mutations in all populations at the end of the simulation.

Model-specific characteristics

After burn-in, populations evolved for 100,000 generations under neutral drift or stabilizing selection, depending on the treatment. Neutral drift entailed no change from the properties of the burn-in, whereas stabilizing selection imposed a fitness function on phenotypes, invoking a multivariate phenotypic optimum a fixed distance from the mean population phenotype post-burn-in. Note that some amount of drift still existed in selection-treated populations due to a finite population size.

The position of the phenotypic optimum is defined as:

$$\Omega = \bar{x} + (\mu\gamma\rho)\bar{x} \quad (2)$$

where \bar{x} is the vector of phenotype means for the population following burn-in, μ is the per-locus, per-generation mutation rate; γ , is the average number of mutational steps to reach the phenotypic optimum, and ρ is the number of generations of burn-in. For my purposes, $\mu = 8.045 \times 10^{-6}$, $\gamma = 100$, and $\rho = 50000$. This distance was

close to the original phenotypes, meaning most of the simulation (approximately 98,000 generations) investigated the maintenance of variation around a phenotypic optimum.

The fitness of an individual in the population was defined as:

$$\omega(i) = 1 - s \left(1 - e^{-\frac{1}{\tau} \sum_{n=1}^n x_n^2} \right), \quad (3)$$

where s is the selection coefficient, τ represents the gradient of the selection curve, n is the number of traits, and x_n is the individual's distance to the optimum for trait n . To ensure a theoretical minimum and maximum fitness, s was fixed at 0.9, ensuring minimum fitness was $1 - s = 0.1$, and maximum fitness was 1. This resulted in individuals at the phenotypic optimum being at most ten times as fit as those infinitely far from the phenotypic optimum. The model-specific maximum fitness difference depends on τ : the larger τ is, the smaller the fitness difference between individuals.

Model Parameterization

Five parameters were shared between models, with a sixth for testing selection (Table 1). These were sampled using a Latin hypercube sampling design (HELTON AND DAVIS 2003), with 1024 parameter combinations testing the null model, and 256 testing the selection model (Figure S3). The hypercube sampling was necessary to explore the parameter space well, as simple factorial designs would have left much of the hyperspace unsampled. Each hypercube sample represents a combination of parameters, with the total set of samples designed to maximize the distance between samples (sampling more of the total space), and minimize correlations between them (sampling that space evenly) (HELTON AND DAVIS 2003). Hypercube samples were generated using the R packages 'DoE.Wrapper' and 'LHS', using the maximin algorithm (R DEVELOPMENTAL CORE TEAM 2019; GROEMPING 2020). Each sample/model was repeated 100 times, using 100 seed values fed to SLiM. These seeds were randomly sampled from a uniform distribution of the total range of unsigned 32-bit integers (1 to $2^{32} - 1$) (R DEVELOPMENTAL CORE TEAM 2019). The array of parameter combinations and replicates was processed across 1152 cores on the University of Queensland's Tinaroo high-performance computing (HPC) system, using

embedded Nimrod scripts to feed parameter/seed combinations to individual SLiM processes. All code has been deposited to a GitHub repository (<https://github.com/nobrien97/Genetic-Architecture-in-SLiM>), and all relevant data to a RDM folder (<https://cloud.rdm.uq.edu.au/index.php/s/mLsz2ngFKKFPWeN> - Password = Hypercube2020). This will be made publicly available upon acceptance of this manuscript in a scientific journal.

Analysis

For analysis, I considered population trait variances, covariances, distances from the optimum, and mutational effects at the final generation of the simulation (100,000). I also tracked trait variances and covariances over time. Trait variances and covariances were pooled and averaged to form a ‘mega-trait’ average variance and covariance, since traits were functionally identical. I computed the population mean Euclidean distance from the phenotypic optimum for each replicate and model:

$$d(\mathbf{p}, \mathbf{q}) = \sqrt{\sum_{i=1}^n (q_i - p_i)^2}$$

Where p_i and q_i are the population mean and phenotypic optimum value, respectively, for trait i .

The interaction between τ and mutation rate was treated as a ‘CoA model’ parameter, indicating whether the hypercube sample approximated House-of-Cards allelic effects, or Gaussian effects. An additional model type, ‘Null’, summarized the models with no selection and any mutation rate. Remaining models with intermediate selection strengths and mutation rates were not considered for analysis, although that remains an exciting prospect for the future. I binned additive effect size variance, recombination rate, pleiotropy rate, and mutational correlation hypercube values into low, medium, and high categories for simpler interpretation.

To determine the effects of CoA model on adaptation, I explored the distribution of final distances from the phenotypic optimum, finding a distinct ‘dead zone’ where distances were not represented by populations. I used this dead zone to classify models into two categories: adapted, or maladapted. Adapted models had distances

from the phenotypic optimum less than 16 phenotypic units, and maladapted with distances greater than 16 phenotypic units. I used a χ^2 test followed by an odds-ratio post-hoc to determine the differences in representation among CoA models in adapted and maladapted categories. Following this, I discarded maladapted populations, choosing to focus on investigating the genetic architectures underlying adapted populations.

To evaluate the effects of genetic architecture on adaptation under the CoA models, I used Eicker-Huber-White (EHW) error multiple regression models to determine the effects of CoA model type, additive effect size, recombination rate, pleiotropy rate, and mutational correlations between traits on distance from the phenotypic optimum, additive variance, and trait covariances. I compared estimated marginal means with Tukey correction to assess differences between Continuum of Alleles models and parameter levels. I also collected the mutational effects of segregating alleles at the end of the simulation. With this, I compared mean distributions of allelic effect sizes in adapted populations according to additive effect variability with EHW-error multivariate multiple regression. Responses included mean allelic effect, variance, and kurtosis of the distribution, as well as the mutation counts contributing to V_A within each model. Multiple regressions investigating allelic distributions were calculated across 50 replicates owing to computer random access memory (RAM) limitations.

Despite not all data conforming to normality, no data was transformed owing to the large sample sizes. Previous work into the robustness of t - and F -tests have shown that departures from normality can usually still provide reliable estimates, provided the number of observations is large enough that coefficient estimates are approximately normally distributed according to the central limit theorem (LUMLEY *et al.* 2002). This was verified with diagnostic tools in the R package “jtools” (LONG 2020). In terms of regression analysis, heteroscedasticity can remain a problem, even with large sample sizes. To account for this, I used Eicker-Huber-White HC2 or HC3 robust standard errors in my linear regression models via the ‘estimatr’ package in R (EICKER 1967; HUBER 1967; WHITE 1980; HAYES AND CAI 2007; BLAIR 2020). Due to the large sample sizes (128,000 total models, 4635 representing adapted populations), I was able to find significant differences between groups with extremely small effect sizes. To ensure I focused only on biologically meaningful differences, I calculated the relative

contributions of parameters to the appropriate regression, using the Lindeman, Merenda and Gold method (LINDEMAN 1980), explaining only the factors that contributed meaningfully to variation.

Results

Tracking population dynamics over time

To determine whether populations were under mutation-selection-drift balance by the end of the simulation, I plotted additive variance and covariance over time across selection strengths. I reasoned that the joint effects of mutation (which creates variance) and drift and selection (which remove variance), would lead to stable levels of genetic variability over long periods of time. I found that after 100,000 generations (two days of model run-time), variance increased asymptotically in all models (Figure 3), suggesting that levels of genetic variability were unlikely to change significantly in longer model runs. As expected, mean additive variance was consistently higher under a Gaussian model, whereas it remained low and almost constant in the House-of-Cards models (Figure 3A). Both selection models clearly behaved differently from a null model where genetic drift was expected to dominate. Owing to mutation rates being averaged across null models, variance was maintained at an intermediate level relative to the high variance Gaussian and low variance House-of-Cards models (Figure 3A). Covariance between traits acted similarly across models (Figure 3B). Knowing that by generation 100,000 models were at mutation-selection-drift equilibrium, I could investigate whether populations were well-adapted under different selection and genetic models.

General patterns of adaptation with Continuum of Alleles models

I explored the distribution of Euclidean distances around a phenotypic optimum under House-of-Cards and Gaussian models of allelic effects and compared them to a null model without selection (Figure 4A). Both Gaussian and House-of-Cards models showed a small proportion of populations that were adapted, coming within 16 phenotypic units from the phenotypic optimum. There was a visible division between these adapted populations and the remaining maladapted populations (Figure 4). The 'dead space' that separated these populations did not exist in the Null model. To

further explore this bimodality, I examined the differences between models in their ability to reach the adapted space (i.e. within 16 phenotypic units from the optimum). Populations were more likely to be found in the adapted zone if they belonged to either selection model over the Null model ($\chi^2 = 9602.1$, $df = 2$, $p < 0.0001$). 15.23% of Gaussian populations reached the adapted space, while House-of-Cards populations reached this space 16.1% of the time. By contrast, 0.53% of Null populations reached the adapted space. A post-hoc odds ratio test found significant differences between Null and Gaussian (OR = 33.566, 95% C.I. = 29.5, 38.2, $p < 0.0001$) and Null and House-of-Cards (OR = 35.872, 95% C.I. = 31.5, 40.85, $p < 0.0001$), but not between Gaussian and House-of-Cards (OR = 1.069, 95% C.I. = 0.93, 1.23, $p = 0.35$).

Genetic architecture effects on adaptation with Continuum of Alleles models

To understand the underlying genetic architectures of populations that were able to come close to the phenotypic optimum, I compared the effects of genetic architecture on distance to the phenotypic optimum (Figure 5; Table 2), mean trait variance (Figure 6), and mean trait covariance (Figure 7) across the two selection models. I compared the effects of varying additive effect sizes, recombination rates, pleiotropy rates, and mutational correlations on Euclidean distances of populations close to the phenotypic optimum under Gaussian or House-of-Cards mutational models. Table 2 shows the mean effects of these variables on how close populations get to the phenotypic optimum (i.e., their adaptedness), as well as the effects on trait variance and covariance. Although all genetic architecture parameters had significant effects on distance, variance and/or covariance, most of these effects were small in magnitude. For brevity, I discuss only the parameters that explain the most variation in these responses. Variation in distance was explained mostly by pleiotropy (explaining 8.6% of total variation among models), model type (explaining 5.4% of variation, and additive effect size (explaining 2.8% of variation). Mean distance from the phenotypic optimum was lowest when additive effect sizes were low (0.841 ± 0.181 ; Figure 4); this did not change between CoA models ($t_{921} = -0.422$, $p = 0.998$). However, House-of-Cards models were more robust to changes in additive effect size than Gaussian models ($t_{921} = -2.583$, $p = 0.01$).

When increasing effect size from low to high under a Gaussian model, adapted populations' mean distance from the phenotypic optimum increased by 2.203 ± 0.232 phenotypic units ($t_{921} = -9.504$, $p < 0.0001$). The same change in effect size under a House-of-Cards model resulted in no significant change in mean distance ($t_{921} = -0.587$, $p = 0.827$). Figure 5 shows how patterns of adaptation varied between Continuum of Alleles models when increasing the variance of allelic effect sizes. Pleiotropy rate increased distance to the optimum; however, there was no interaction between pleiotropy and model type ($t_{921} = 0.843$, $p = 0.399$). Increasing pleiotropy rate from low to high led to an average 1.261 ± 0.178 unit decrease in distance from the phenotypic optimum ($t_{921} = 7.099$, $p < 0.0001$). These effects on distance were not always mirrored with the effects of genetic architecture on trait variance, which was explained by additive effect size (45.1% of variation in trait variance) and its interaction with model type (explaining 14.4% of this variation).

On average, House-of-Cards models near the phenotypic optimum had considerably more additive variance than Gaussian models (40.4 ± 18.72 units vs 2.6 ± 0.07 units; $t_{921} = -2.019$, $p = 0.044$). Under a Gaussian model, increasing the additive effect size of populations in the adapted zone marginally increased trait variance ($t_{921} = -14.386$, $p < 0.0001$; Figure 5A), however, this was not the case under a House-of-Cards model ($t_{921} = -1.958$, $p = 0.123$). Figure 6 shows how additive effect size interacts with Gaussian and House-of-Cards models to drive differences in variance in adapted populations. Note that several outliers were removed from Figures 6 and 7 owing to their distortion of the figures. These outliers had variance greater than 50 and covariance less than -5 (Figure S3, S4). Similarly to variance, differences in covariance could be explained mainly by differences in additive effect size (explaining 46.4% of variation), and the interaction between effect size and the Continuum of Alleles model type (explaining 15.6% of variation).

Average trait covariance differed between models ($t_{921} = 2.147$, $p = 0.032$; Figure 6), with Gaussian models carrying very little genetic covariance amongst traits (covariance = 0.014 ± 0.005), and House-of-Cards models carrying slightly more (covariance = -3.616 ± 1.691). Increasing additive effect size from lower to higher levels in Gaussian models led to slight declines in covariance (a decrease of 0.039 ± 0.005 ; $t_{921} = 7.526$, $p < 0.0001$; Figure 6A). No significant effect of increasing additive effect size on covariance was seen in House-of-Cards models ($t_{921} = 1.937$, $p = 0.129$).

However, the difference in response to additive effect size between models was marginally insignificant ($t_{921} = -1.929$, $p = 0.054$). Figure 7 shows the effects of increasing additive effect variance and Continuum of Alleles model type on covariance.

These analyses suggest that additive variance and covariance are rather robust under House-of-Cards models, and less so under Gaussian models. Additive effect size variability in particular is important for understanding the interplay between adaptation and additive variance. I compared the proportions of CoA models that reached the phenotypic optimum according to their additive effect size variance, finding 36.12% of low additive effect variance models were adapted, versus 2.29% of medium-variance populations, and 0.19% of large-effect, high-variance populations ($\chi^2 = 1572.13$, $df = 2$, $p < 0.0001$). While a significant interaction between additive effect size variability and model type occurred ($\chi^2 = 8.571$, $df = 2$, $p = 0.0138$), this was not meaningful – the differences in probability to reach the phenotypic optimum were miniscule, as shown in Figure S4.

Allelic effect size distributions with Continuum of Alleles models

To analyze the underlying cause of these variances, covariances, and by extension, distances to the phenotypic optimum, study of the underlying allelic effect size distributions of the models proved illuminating. I compared the means, variances, kurtosis, and count of mutations contributing to these distributions across models to understand the mutational limitations imposed by genetic architectures under the two CoA models.

The distributions of allelic effects can be characterized by several moments: the mean of the effects, which might be biased in some direction by genetic architectures; the variance of the distribution, indicating the effect size variability in segregating mutations; and the kurtosis of the distribution, indicating the rarity of large-effect alleles. As with the prior analyses, additive effect size and model type explained most variability in these distributional statistics. I will focus on the effects which explain the most variability in model space. For the effects of the less influential parameters, refer to Table 3. To assess the mutational bias of models, I first compared the means of distributions across models and genetic architectures. Since the resulting

regression indicated a lack of directional mutational bias ($F_{17, 411} = 1.127$, $p = 0.325$, Adjusted $R^2 = 0.189$), I turned my attention to the variance of distributions to understand the constraints that genetic architectures might apply to populations trying to hover around an optimum. Additive effect size explained 66.2% of total variability between models ($F_{17, 411} = 55.04$, $p < 0.0001$, Adjusted $R^2 = 0.851$). Under a Gaussian model, increasing additive effect size from low to medium significantly increased allelic effect variance by 6.02 ± 0.372 phenotypic units ($t_{411} = -16.188$, $p < 0.0001$; Figure 8). However, no significant difference occurred for increasing variance from low to high or from medium to high. No significant changes to variance with increasing effect size were observed under House-of-Cards models. Figure 8 shows the distributions of allelic effects with changing additive effect size variability under Gaussian and House-of-Cards models.

Kurtosis, which describes the rarity of large-effect alleles, differed significantly across models and genetic architectures with additive effect size variance explaining 31.9% of variability between models, and the interaction between additive effect size and model type contributing another 15.5% ($F_{17, 411} = 12.36$, $p < 0.0001$, Adjusted $R^2 = 0.6$). Under the Gaussian model, increasing additive effect size from low to medium increased kurtosis by 0.985 ± 0.159 ($t_{411} = -6.206$, $p < 0.0001$). No analogous effect was seen under the House-of-Cards model ($t_{411} = -0.944$, $p = 0.6130$). As well as the distributions of allelic effects, the absolute counts of mutations contributing to each distribution gives an indicator of the genetic diversity of populations.

To assess the effects of genetic architecture and models on limiting the number of segregating alleles, I compared mutation counts between models, finding significant differences among models ($F_{17, 411} = 580.2$, $p < 0.0001$, Adjusted $R^2 = 0.94$). Model type contributed the most to explaining mutation count variation among models, describing 58.4% of among-model variation. Pleiotropy rate explained 10% of variation, however, this is explicated by each pleiotropic mutation contributing multiple effects with a single mutation. The mean number of mutations in Gaussian models was considerably higher than that of House-of-Cards models, but over a large range of values: 1516 ± 6608 mutations for Gaussian models versus 374 ± 114 for House-of-Cards ($t_{411} = 0.173$, $p = 0.863$).

Discussion

My findings show that populations under Gaussian (high mutation rate, weak selection) or House-of-Cards (low mutation rate, strong selection) models can adapt to phenotypic optima under stabilizing selection, however, the chance of doing so is quite low (16.1% of House-of-Cards populations reached distances within the adapted space, along with 15.23% of Gaussian populations; Figure 4A). Hence, maladaptation seems quite common, at least under a population size of 8000 and the associated levels of drift. This supports previous predictions of maladaptation prevalence: maladaptation should be common given the capacities of selection, drift, and inbreeding depression to remove additive variation, and hence reduce the ability of populations to respond quickly to environmental changes (CRESPI 2000; AGUIRRE *et al.* 2014; BRADY *et al.* 2019). Among maladapted populations, House-of-Cards and Gaussian models had high variability in their final distance to the phenotypic optimum (Figure 4A), comparable to null models. In these populations, drift likely overcame selection, locking populations under a drift-barrier (LYNCH *et al.* 2016).

Drift-barriers arise when weakly selected loci are unable to overcome the strength of drift (LYNCH *et al.* 2016; GARDON *et al.* 2020). This problem is especially prevalent in small populations where drift is expected to dominate. However, large populations can also experience this if selection pressures on affected loci are weak enough (LYNCH 2010; GARDON *et al.* 2020). Evidence for drift-barriers is scarce in natural populations, however, Gardon *et al.* (2020) found relaxed selection in genes inherited from small ancestral clades in *Prochlorococcus marinus*, a marine cyanobacterium. In comparison, evidence for strong negative selection was found in more recent *P. marinus* genes, arising in a much larger derived population (GARDON *et al.* 2020). Taken together, these differences in selection across gene sets indicates a drift-barrier model for evolution (LYNCH *et al.* 2016; GARDON *et al.* 2020). The large variability in distances from the phenotypic optimum in maladapted populations here is analogous to Gardon's findings, indicating strong drift among both House-of-Cards and Gaussian populations. Since most traits are reasonably well adapted in nature (ORR 1998), selection must be relatively strong relative to drift to drive populations away from mildly maladapted phenotypes, particularly if population sizes are small.

In quantitative genetics theory, the infinitesimal limit is analogous to the drift-barrier. Under the infinitesimal model, infinitely many loci have an infinitely small effect on trait values (FISHER 1918). This means that selection is weak relative to drift, as in the drift-barrier model (ROBERTSON 1960). Under the infinitesimal limit, variance is expected to be unaffected by selection: drift overcomes selection on a per-locus basis and is able to randomly fix alleles (BARTON 2017). As shown in Figure 4A, maladapted populations in both Gaussian and House-of-Cards populations were highly variable, indicating that they likely represent this limitation of selection.

Even among adapted populations, the effect of the drift-barrier/infinitesimal limit might be pronounced in future responses to selection. Houle (1998) pointed out that selection can cause spatial variation in effective population size across the genome by removing genetic variation. In turn, this reduces the adaptability of populations and increases the strength of drift (LEIGH 1970; AGASHE *et al.* 2011; BATESON 2017). While the strength of selection seems necessary for driving adaptation past drift-barriers, I found no significant difference in the number of House-of-Cards (strong selection) and Gaussian (weak selection) populations that reached the phenotypic optimum. Selection alone is not enough: mutational input must provide the variation for selection to act on without swamping the population with strongly deleterious large-effect alleles (FISHER 1930; FRANSEN *et al.* 2017).

In tandem with selection strength, mutation rate defines the differences between Gaussian and House-of-Cards models (WALSH AND LYNCH 2018). Gaussian models have higher mutation rates relative to selection strength (LANDE 1975). This raises the expectation that Gaussian models should maintain more variability following adaptation and carry more mutations of small effect (HODGINS-DAVIS *et al.* 2015; WALSH AND LYNCH 2018). This is contrasted by the House-of-Cards model where strong selection paired with low mutation rates allows for intermediate-sized effects to rise in frequency without the population being swamped by many more common variants (TURELLI 1984; HODGINS-DAVIS *et al.* 2015). The variation in the size of mutational input is therefore extremely important to the expectations of these models: Gaussian models are expected to function with small effect sizes, while House-of-Cards are assumed to function by selecting moderately-sized alleles (TURELLI 1984; WALSH AND LYNCH 2018). Adjusting effect size variation has implications for the

efficacy of adaptation under these different models since Gaussian and House-of-Cards models are not equally sensitive to changes in effect size variation.

House-of-Cards models were generally robust to changes in additive effect size, with distance from the phenotypic optimum, variance, and covariance remaining similar across effect size variation treatments (Figure 5 – 7). Gaussian models on the other hand were perturbed by increases to mutational effects, with wider distributions and more maladaptation occurring under high mutational variance scenarios. This is due to differences in selection strengths between models. While at the phenotypic optimum, most new mutations are deleterious under House-of-Cards models (TURELLI 1984): the strong selective pressure on these populations leads to a constant mutational load that is unchanged by increasing mutational variance (Figure 8, Table 3). In other words, new large-effect mutations that move populations away from the phenotypic optimum are efficiently removed from the population regardless of their relative rarity (Figure 6). In contrast, under Gaussian models, increasing mutational variance creates large-effect mutations that are less deleterious and more common (HODGINS-DAVIS *et al.* 2015). Hence, large-effect mutations are able to persist in greater numbers, driving increases in variance in the distance to the optimum (HODGINS-DAVIS *et al.* 2015). House-of-Cards models then show increased adaptedness over time, with closer adherence to the phenotypic optimum relative to Gaussian models (Figure 5, 8). Like molecules at lower temperatures, ‘cold’ House-of-Cards populations do not move as erratically as ‘hot’ Gaussian populations.

The phenotypic volatility of populations under high-variance mutation has implications for adaptation to new environments. For example, simulations by Gilbert and Whitlock (2017) showed that adaptation could occur through genetic architectures containing many genes of small-effect or few genes of large-effect. However, adaptation in the populations under the few-genes-large-effect architecture took longer to achieve (GILBERT AND WHITLOCK 2017). In addition, they found that adaptation could succeed under two cases: (1) the classical example, where high genetic variation and small-effect alleles drive adaptation; and (2), where genetic variation might be low, but there are sufficient large-effect alleles to drive adaptation (GILBERT AND WHITLOCK 2017). If Gaussian populations move towards a phenotypic optimum with high additive effect size variability, they fall in the middle of this: high expected additive variance from higher mutation rates (WALSH AND LYNCH 2018) and

many large-effect alleles that aid in the initial directional push towards a phenotypic optimum (ZHANG 2012). Thus, rapid movement towards the phenotypic optimum is expected. However, these large effects might become a liability once the population arrives at the phenotypic optimum.

Large effect alleles are likely to lower population fitness considerably under Gaussian models post-adaptive walk (WALSH AND LYNCH 2018). With small-effect mutations, adaptation is likely to be slower (GILBERT AND WHITLOCK 2017), but maladaptation post-walk will be considerably weaker: it will take many more mutations to move the population away from the phenotypic optimum the same amount as a single large-effect mutation. The weak-selection-high-mutation-rate paradigm of Gaussian regimes is critical to their response to varying effect sizes, however, under House-of-Cards models robustness against increased mutational variance is expected when populations are at a phenotypic optimum.

Under a House-of-Cards model, populations face stronger selection relative to mutation rates (TURELLI 1984), meaning that adaptation is driven by mutational variance rather than standing genetic variation (WALSH AND LYNCH 2018). While populations are at a phenotypic optimum, mutations are likely to be deleterious, pulling populations towards maladaptation. Under House-of-Cards, mutation rates are low, reducing the chance of this happening. Furthermore, selection is strong: should a large-effect mutation arise in populations hovering around a phenotypic optimum, it is likely to be removed from the population quickly (ZHANG 2012). This means that regardless of the mutational input and the stochastic effects of moderate drift, House-of-Cards populations can efficiently remove deleterious alleles, maintaining their position in phenotypic space more effectively than the 'hotter' Gaussian models.

To illustrate this theory, Figure 9 represents the adherence of populations to a phenotypic optimum given their genetic architecture and Continuum of Alleles assumptions. Gaussian populations are poor at self-regulating mutational distributions due to weak selection being unable to effectively purge the large amount of deleterious mutations entering the population each generation. Under small effect sizes, Gaussian populations can therefore reach the phenotypic optimum, but they are more likely to become maladapted over time, due to the inefficiency of selection in removing weakly-deleterious mutations and the effect of the drift-barrier (OHTA 1973; LYNCH *et al.* 2016).

House-of-Cards models on the other hand can maintain their mutational distributions, withstanding high mutational variability without being swamped by overwhelming numbers of large-effect mutations (Figure 8, 9, Table 9). Hence there is a trade-off: Gaussian models might be able to bring populations to the phenotypic optimum quickly by using standing variation (GILBERT AND WHITLOCK 2017), however, under large additive effect regimes these populations are more likely to be maladapted – that is, greater than 16 phenotypic units from the phenotypic optimum in my simulations. This pattern is illustrated in Figure 1, where highly variable populations are likely to quickly reach their local phenotypic optimum, but unlikely to hover around it closely. House-of-Cards models might adhere to the phenotypic optimum more closely, however, due to the reliance on new mutations, it will take longer for them to reach the phenotypic optimum. Evidence for similar adaptability-adaptedness trade-offs exist in gene networks. Malcom (2011) found that a trade-off between adaptive accuracy and speed of adaptation occurred in a simulation between two species competing in a variable environment. Smaller gene networks produced a competitive advantage in more temporally variable environments, whereas large gene networks resulted in increased accuracy when environments were more stable over time (MALCOM 2011). Similarly, tropical diatom species have shown the ability to quickly adapt to increasing ocean temperatures, at the cost of reducing their photosynthetic efficiency and growth rate (JIN AND AGUSTI 2018). But which side of this adaptability versus adaptedness (LEIGH 1970) trade-off is most advantageous?

In spatially and/or temporally heterogeneous environments, Gaussian models should fare better than House-of-Cards: the rapid evolution towards the phenotypic optimum offsets any accuracy costs, as these inaccuracies will be nullified by a new range shift and could contribute to driving populations towards a new local phenotypic optimum (MALCOM 2011). Indeed, it has been well-documented that higher mutation rates can evolve due to environmental stressors (LENSKI AND SNIEGOWSKI 1995; SNIEGOWSKI *et al.* 1997). Bacterial populations under antibiotic stress have been shown to evolve hypermutability via mutator phenotypes (CAIRNS *et al.* 2017). In eukaryotes, Mutator transposable elements (MULEs) appear common in both parasites and plant hosts, potentially due to the “two-speed genomes” hypothesis, where repeat-rich genomic regions evolve quickly via regulatory changes, in contrast to gene-rich regions that evolve more slowly (DUPEYRON *et al.* 2019). An example for

this mattering for adaptation is in coevolution, where the dichotomy between gene-rich and repeat-rich regions hastens the coevolutionary arms race between parasite and host species (EHRlich AND RAVEN 1964; DUPEYRON *et al.* 2019). Simulations support these empirical findings, with mutation rates depending on the degree of environmental variability (GILLESPIE 1981).

The greater additive variance introduced by increased mutation rates (WALSH AND LYNCH 2018) could also provide Gaussian populations with a ‘head-start’ to begin adaptation quickly after an environmental event (MALCOM 2011) or a greater ability to radiate to new niches in the case of spatial environmental variation (MARQUES *et al.* 2019). In fact, under spatial gradients, highly variable effect sizes could seed populations with variation that allows their members to colonize differential micro-environments (KAGAWA AND TAKIMOTO 2018). In addition, the propensity of drift to drive populations away from phenotypic optima might not be as problematic in heterogeneous environments. Wright (1931; 1932) proposed an interaction between drift, stabilizing selection, and migration where random changes in allele frequencies due to drift could lead to the exploration of trait space away from the phenotypic optimum. If the optimum moves, this variability could become beneficial, leading to rapid movement towards the new optimum (DE VLADAR AND BARTON 2014).

An alternative to note is phenotypic plasticity, where the problem of increased mutational load is diminished by a single genotype leading to multiple phenotypes which can be activated in response to a changing environment (SCHLICHTING 1986). However, there are limits to plasticity (MURREN *et al.* 2015) and it can inhibit future adaptation, increasing populations’ susceptibility to extinction following a large environmental shift (OOSTRA *et al.* 2018). Hence, there are likely situations where plasticity cannot evolve (VAN KLEUNEN AND FISCHER 2005) and adaptation by mutation is necessary. In more homogeneous environments, where any movement from the current phenotype tends to be deleterious, House-of-Cards models should be favored.

Populations evolving by strong selection and low mutation should be advantaged in static environments. Without environmental change to perturb the phenotypic optimum, almost all trait mutations are deleterious, moving populations away from the phenotypic optimum (MATIC *et al.* 1997; WALSH AND LYNCH 2018). Hence, the genetic load felt by populations under Gaussian models would be greater

than that of House-of-Cards models under a stable environment. The finer control that House-of-Cards mutation-selection balances have on allelic frequencies (Figure 8) allows for a better fit to the phenotypic optimum over the long term, at the cost of slower adaptation to new environments (due to relying on new mutational variance to drive adaptation) (MALCOM 2011; WALSH AND LYNCH 2018). In addition, lower mutation rates mean that populations consume less energy maintaining an adapted state relative to Gaussian populations, due to the costs of removing deleterious alleles from the population (LAN *et al.* 2012). This explains the ‘colder’, less reactive behavior of adapted House-of-Cards models relative to Gaussian models (Figure 3, 5 – 9).

A limitation of both Gaussian and House-of-Cards models is that they cannot explain observed levels of genetic variation (WALSH AND LYNCH 2018). One explanation for this is that a form of balancing selection on a pleiotropically linked trait accounts for the maintenance of polymorphisms over time (TURELLI AND BARTON 2004). Under balancing selection, the most fit genotypes at a single locus are polymorphic, either through overdominance (heterozygote-advantage), or rare-allele-favored frequency-dependent selection (CHARLESWORTH 2006). In this case, frequency-dependent selection is a likely explanation, given that my models involve no dominance, and that stabilizing selection on traits means that the fitness effects of alleles at some locus are dependent on the allele frequencies of other loci (FISHER 1930). Predictions state that variation can only be maintained at loci where the aggregate strength of balancing selection is stronger than that of stabilizing selection (BARTON 1990). However, this would reduce the signal of stabilizing selection on traits (BARTON 1990), which is clearly seen in Figure 8, with normal distributions of allelic effects. Hence, balancing selection is unlikely to be maintaining variance in adapted populations here, and the levels of variation reflect that: low variance is seen across almost all adapted populations (Table 2).

While additive effect size had strong effects on models, quantitative genetics theory also has predictions for the effects of pleiotropy, recombination, and mutational correlations that were either absent or weak in my simulations (Table 2). This could be due to differences between expectations while maintaining variation post-adaptation versus approaching the phenotypic optimum on the adaptive walk itself (WALSH AND LYNCH 2018). Zhang and Hill (2002) found that the genetic variance maintained in a population depended very little on pleiotropy, and more so on the

strength of realized stabilizing selection. While recombination is expected to increase additive variation (BARTON AND CHARLESWORTH 1998) and reduce covariation among traits (LANDE 1975), the parameterization might have been too narrow to see this effect over the much larger effect of additive effect size variation.

Among the limitations of the simulations here are the chosen ranges of several parameters. While efforts were made to choose biologically meaningful ranges (Table 1), it was not always possible owing to performance restrictions. Simulations took around 2 days to complete each and although models were run in parallel on a multi-node computing cluster, limitations on computer resource availability led to me sampling a smaller parameter space than originally intended. Recombination rate was sampled from 0 to 9.22×10^{-8} cM/Mb, which is a relatively high recombination rate in plants (STAPLEY *et al.* 2017). However, this rate is low in comparison to some of the recombination rates in other taxa. For example, recombination rates in fungi can reach upwards of 100 cM/Mb (STAPLEY *et al.* 2017). I was unable to vary population size due to difficulties in effectively sampling a larger-dimensional hyperspace with the time necessary to run simulations, and with the increased computational requirements associated with increasing population sizes in individual-based models (HALLER AND MESSER 2019). My implementation of a mega-trait also limits insight into mutational correlations among traits and the effect of pleiotropy. Since fitness effects were identical across traits, the effects of pleiotropy and mutational correlation would be averaged across traits, minimizing the signal. These limitations highlight exciting expansions of my methodology in the future.

I have produced a framework to understand polygenic adaptation in the context of both quantitative and population genetics and genomics. Expanding this model to explain differences in the effects of drift in mutation-selection balance models would lend insight into the effects of heightened drift-barriers on restricting adaptation under models with varying degrees of mutational variance and selection strength. Varying the number of loci contributing to traits could also reveal the robustness of variation under changing polygenicity. Variation in population size would reveal the importance of the drift-barrier in limiting adaptation. Fitness differences among traits would allow for more realistic studies of variance and covariance with additive genetic variance-covariance matrices, **G** matrices (LANDE 1979). Recent developments in **G** matrix analysis involving eigentensor decomposition of sets of matrices (HINE *et al.* 2009;

AGUIRRE *et al.* 2014) have been successful in determining differences in multivariate variation between populations (WALTER *et al.* 2018), which seems promising for comparisons between genetic architectures. Decreasing the number of traits might also increase adaptability, owing to the cost of complexity (ORR 2000). While here I have explored the maintenance of variation, a natural progression is to quantify how these models differ in their adaptive walks, carefully exploring the conjecture of an adaptedness-versus-adaptability trade-off in polygenic adaptation. Similarly, integrating moving phenotypic optima and heterogeneous environments into the model will test the predictions of where Gaussian and House-of-Cards mutation-selection balances are expected to be advantageous.

Overall, this study has shown that the dynamics of House-of-Cards and Gaussian mutation-selection-drift balance models are clearly affected by mutational effect sizes differently, suggesting trade-offs between adaptability and adaptedness are common. Further analysis of these trade-offs with respect to the dynamics of CoA models might help us understand why maladaptation appears so prevalent in natural populations.

Acknowledgments

I would like to thank D. Ortiz-Barrientos, and J. Engelstaedter for their help with constructing these models and their support throughout Honours. I would also like to thank the members of the Ortiz-Barrientos Lab, especially M. James, Z. Broad, and A. Kaur, for their support and feedback on early revisions of this document. This research was funded in part by the Australian Research Council.

References

- Agashe, D., J. J. Falk and D. I. Bolnick, 2011 Effects of founding genetic variation on adaptation to a novel resource. *Evolution* 65: 2481-2491.
- Aguirre, J. D., E. Hine, K. McGuigan and M. W. Blows, 2014 Comparing G: multivariate analysis of genetic variation in multiple populations. *Heredity* 112: 21-29.
- Albert, A. Y., S. Sawaya, T. H. Vines, A. K. Knecht, C. T. Miller *et al.*, 2008 The genetics of adaptive shape shift in stickleback: pleiotropy and effect size. *Evolution* 62: 76-85.
- Aston, E., A. Channon, R. V. Belavkin, D. R. Gifford, R. Krasovec *et al.*, 2017 Critical Mutation Rate has an Exponential Dependence on Population Size for Eukaryotic-length Genomes with Crossover. *Scientific Reports* 7: 15519.
- Barghi, N., J. Hermisson and C. Schlotterer, 2020 Polygenic adaptation: a unifying framework to understand positive selection. *Nature Reviews Genetics*.
- Barton, N. H., 1990 Pleiotropic models of quantitative variation. *Genetics* 124: 773-782.
- Barton, N. H., 2017 How does epistasis influence the response to selection? *Heredity (Edinb)* 118: 96-109.
- Barton, N. H., and B. Charlesworth, 1998 Why sex and recombination? *Science* 281: 1986-1990.
- Barton, N. H., A. M. Etheridge and A. Veber, 2017 The infinitesimal model: Definition, derivation, and implications. *Theoretical Population Biology* 118: 50-73.
- Bateson, P., 2017 Adaptability and evolution. *Interface Focus* 7: 20160126.
- Author, 2020 estimatr: Fast Estimators for Design-Based Inference. 0.26.0, <https://CRAN.R-project.org/package=estimatr>
- Brady, S. P., D. I. Bolnick, A. L. Angert, A. Gonzalez, R. D. H. Barrett *et al.*, 2019 Causes of maladaptation. *Evolutionary Applications* 12: 1229-1242.
- Cairns, J., J. Frickel, M. Jalasvuori, T. Hiltunen and L. Becks, 2017 Genomic evolution of bacterial populations under coselection by antibiotics and phage. *Molecular Ecology* 26: 1848-1859.
- Chantepie, S., and L.-M. Chevin, 2020 How does the strength of selection influence genetic correlations? *bioRxiv*.
- Charlesworth, B., 1993 Directional selection and the evolution of sex and recombination. *Genetics Research* 61: 205-224.
- Charlesworth, B., and D. Charlesworth, 2010 *Elements of Evolutionary Genetics*. Roberts and Company, Greenwood Village, Colorado, USA.
- Charlesworth, D., 2006 Balancing selection and its effects on sequences in nearby genome regions. *PLoS Genetics* 2: e64.
- Chesmore, K., J. Bartlett and S. M. Williams, 2018 The ubiquity of pleiotropy in human disease. *Human Genetics* 137: 39-44.

- Crespi, B. J., 2000 The evolution of maladaptation. *Heredity (Edinb)* 84 (Pt 6): 623-629.
- Darwin, C., 1859 *On the origin of species by means of natural selection, or, The preservation of favoured races in the struggle for life*. J. Murray, London.
- de Vladar, H. P., and N. Barton, 2014 Stability and response of polygenic traits to stabilizing selection and mutation. *Genetics* 197: 749-767.
- Dupeyron, M., K. S. Singh, C. Bass and A. Hayward, 2019 Evolution of Mutator transposable elements across eukaryotic diversity. *Mobile DNA* 10: 12.
- Ehrlich, P. R., and P. H. Raven, 1964 Butterflies and Plants - a Study in Coevolution. *Evolution* 18: 586-608.
- Eicker, F., 1967 Limit theorems for regressions with unequal and dependent errors, pp. 59-82 in *Proceedings of the Fifth Berkeley Symposium on Mathematical Statistics and Probability, Volume 1: Statistics*. University of California Press, Berkeley, CA.
- Estes, S., and S. J. Arnold, 2007 Resolving the paradox of stasis: Models with stabilizing selection explain evolutionary divergence on all timescales. *American Naturalist* 169: 227-244.
- Falconer, D. S. M., T. F. C., 1996 *Introduction to Quantitative Genetics*. Pearson Education Limited, Longmans Green, Harlow, Essex, UK.
- Fisher, R. A., 1918 The correlation between relatives on the supposition of Mendelian inheritance. *Transactions of the Royal Society of Edinburgh* 52: 399-433.
- Fisher, R. A., 1930 *The genetical theory of natural selection*. The Clarendon press, Oxford, UK.
- Fleming, W. H., 1979 Equilibrium Distributions of Continuous Polygenic Traits. *Siam Journal on Applied Mathematics* 36: 148-168.
- Franssen, S. U., R. Kofler and C. Schlotterer, 2017 Uncovering the genetic signature of quantitative trait evolution with replicated time series data. *Heredity (Edinb)* 118: 42-51.
- Gardon, H., C. Biderre-Petit, I. Jouan-Dufournel and G. Bronner, 2020 A drift-barrier model drives the genomic landscape of a structured bacterial population. *Molecular Ecology*.
- Gilbert, K. J., and M. C. Whitlock, 2017 The genetics of adaptation to discrete heterogeneous environments: frequent mutation or large-effect alleles can allow range expansion. *Journal of Evolutionary Biology* 30: 591-602.
- Gillespie, J. H., 1981 Mutation Modification in a Random Environment. *Evolution* 35: 468-476.
- Author, 2020 DoE.wrapper: Wrapper Package for Design of Experiments Functionality. 0.11, <https://CRAN.R-project.org/package=DoE.wrapper>
- Haller, B. C., and P. W. Messer, 2019 SLiM 3: Forward Genetic Simulations Beyond the Wright-Fisher Model. *Molecular Biology and Evolution* 36: 632-637.
- Haller, B. C. M., P. W., 2016 SLiM: An Evolutionary Simulation Framework.

- Hayes, A. F., and L. Cai, 2007 Using heteroskedasticity-consistent standard error estimators in OLS regression: An introduction and software implementation. *Behavior Research Methods* 39: 709-722.
- Helton, J. C., and F. J. Davis, 2003 Latin hypercube sampling and the propagation of uncertainty in analyses of complex systems. *Reliability Engineering & System Safety* 81: 23-69.
- Hill, W. G., and A. Robertson, 1966 Effect of Linkage on Limits to Artificial Selection. *Genetics Research* 8: 269-294.
- Hine, E., S. F. Chenoweth, H. D. Rundle and M. W. Blows, 2009 Characterizing the evolution of genetic variance using genetic covariance tensors. *Philosophical Transactions of the Royal Society B: Biological Sciences* 364: 1567-1578.
- Hodgins-Davis, A., D. P. Rice and J. P. Townsend, 2015 Gene Expression Evolves under a House-of-Cards Model of Stabilizing Selection. *Molecular Biology and Evolution* 32: 2130-2140.
- Houle, D., 1998 How should we explain variation in the genetic variance of traits? *Genetica* 102-103: 241-253.
- Houle, D., G. H. Bolstad, K. van der Linde and T. F. Hansen, 2017 Mutation predicts 40 million years of fly wing evolution. *Nature* 548: 447-450.
- Huber, P. J., 1967 The behavior of maximum likelihood estimates under nonstandard conditions, pp. 221-233 in *Proceedings of the Fifth Berkeley Symposium on Mathematical Statistics and Probability, Volume 1: Statistics*. University of California Press, Berkeley, CA.
- Jin, P., and S. Agusti, 2018 Fast adaptation of tropical diatoms to increased warming with trade-offs. *Scientific Reports* 8: 17771.
- Kagawa, K., and G. Takimoto, 2018 Hybridization can promote adaptive radiation by means of transgressive segregation. *Ecology Letters* 21: 264-274.
- Kimura, M., 1965 A stochastic model concerning the maintenance of genetic variability in quantitative characters. *Proc Natl Acad Sci U.S.A* 54: 731-736.
- Kimura, M., 1967 On Evolutionary Adjustment of Spontaneous Mutation Rates. *Genetical Research* 9: 23-34.
- Kimura, M., and J. F. Crow, 1964 The Number of Alleles That Can Be Maintained in a Finite Population. *Genetics* 49: 725-738.
- LaBar, T., and C. Adami, 2017 Evolution of drift robustness in small populations. *Nature Communications* 8: 1012.
- Lan, G., P. Sartori, S. Neumann, V. Sourjik and Y. Tu, 2012 The energy-speed-accuracy tradeoff in sensory adaptation. *Nature Physics* 8: 422-428.
- Lande, R., 1975 The maintenance of genetic variability by mutation in a polygenic character with linked loci. *Genetics Research* 26: 221-235.
- Lande, R., 1976 Natural-Selection and Random Genetic Drift in Phenotypic Evolution. *Evolution* 30: 314-334.
- Lande, R., 1979 Quantitative Genetic-Analysis of Multivariate Evolution, Applied to Brain - Body Size Allometry. *Evolution* 33: 402-416.

- Lande, R., and S. Shannon, 1996 The role of genetic variation in adaptation and population persistence in a changing environment. *Evolution* 50: 434-437.
- Lasky, J. R., 2019 Eco-evolutionary community turnover following environmental change. *Evolutionary Applications* 12: 1434-1448.
- Le Corre, V., and A. Kremer, 2012 The genetic differentiation at quantitative trait loci under local adaptation. *Molecular Ecology* 21: 1548-1566.
- Leigh, E. G., 1970 Natural Selection and Mutability. *American Naturalist* 104: 301-305.
- Lenski, R. E., and P. D. Sniegowski, 1995 "Adaptive mutation": the debate goes on. *Science* 269: 285-288.
- Lewontin, R. C., 1970 The units of selection. *Annual review of ecology and systematics*: 1-18.
- Lindeman, R. H. M., P.F. Gold, R.Z., 1980 *Introduction to Bivariate and Multivariate Analysis*. Scott, Foresman, Glenview, IL.
- Author, 2020 jtools: Analysis and Presentation of Social Scientific Data. 2.1.0, <https://CRAN.R-project.org/package=jtools>
- Lumley, T., P. Diehr, S. Emerson and L. Chen, 2002 The importance of the normality assumption in large public health data sets. *Annual Review of Public Health* 23: 151-169.
- Lynch, M., 2010 Evolution of the mutation rate. *Trends in Genetics* 26: 345-352.
- Lynch, M., M. S. Ackerman, J. F. Gout, H. Long, W. Sung *et al.*, 2016 Genetic drift, selection and the evolution of the mutation rate. *Nature Reviews Genetics* 17: 704-714.
- Lynch, M., and W. Gabriel, 1983 Phenotypic evolution and parthenogenesis. *The American Naturalist* 122: 745-764.
- Lynch, M., and W. Gabriel, 1990 Mutation Load and the Survival of Small Populations. *Evolution* 44: 1725-1737.
- Lynch, M., and R. Lande, 1998 The critical effective size for a genetically secure population. *Animal Conservation* 1: 70-72.
- Malcom, J. W., 2011 Evolution of Competitive Ability: An Adaptation Speed vs. Accuracy Tradeoff Rooted in Gene Network Size. *Plos One* 6.
- Marques, D. A., J. I. Meier and O. Seehausen, 2019 A Combinatorial View on Speciation and Adaptive Radiation. *Trends in Ecology & Evolution* 34: 531-544.
- Matic, I., 2019 Mutation Rate Heterogeneity Increases Odds of Survival in Unpredictable Environments. *Molecular Cell* 75: 421-425.
- Matic, I., M. Radman, F. Taddei, B. Picard, C. Doit *et al.*, 1997 Highly variable mutation rates in commensal and pathogenic *Escherichia coli*. *Science* 277: 1833-1834.
- Murren, C. J., J. R. Auld, H. Callahan, C. K. Ghalambor, C. A. Handelsman *et al.*, 2015 Constraints on the evolution of phenotypic plasticity: limits and costs of phenotype and plasticity. *Heredity (Edinb)* 115: 293-301.

- Nesse, R. M., 2005 Maladaptation and natural selection. *The Quarterly Review of Biology* 80: 62-70.
- Ohta, T., 1973 Slightly Deleterious Mutant Substitutions in Evolution. *Nature* 246: 96-98.
- Oostra, V., M. Saastamoinen, B. J. Zwaan and C. W. Wheat, 2018 Strong phenotypic plasticity limits potential for evolutionary responses to climate change. *Nature Communications* 9: 1005.
- Orr, H. A., 1998 The Population Genetics of Adaptation: The Distribution of Factors Fixed during Adaptive Evolution. *Evolution* 52: 935-949.
- Orr, H. A., 2000 Adaptation and the cost of complexity. *Evolution* 54: 13-20.
- Ortiz-Barrientos, D., J. Engelstadter and L. H. Rieseberg, 2016 Recombination Rate Evolution and the Origin of Species. *Trends in Ecology & Evolution* 31: 226-236.
- Otto, S. P., 2009 The Evolutionary Enigma of Sex. *American Naturalist* 174: S1-S14.
- Author, 2019 R: A language and environment for statistical computing. <https://www.r-project.org/>
- Robertson, A., 1960 A Theory of Limits in Artificial Selection. *Proceedings of the Royal Society Series B-Biological Sciences* 153: 235-249.
- Schlichting, C. D., 1986 The Evolution of Phenotypic Plasticity in Plants. *Annual Review of Ecology and Systematics* 17: 667-693.
- Sniegowski, P. D., P. J. Gerrish and R. E. Lenski, 1997 Evolution of high mutation rates in experimental populations of *E. coli*. *Nature* 387: 703-705.
- Stapley, J., P. G. D. Feulner, S. E. Johnston, A. W. Santure and C. M. Smadja, 2017 Variation in recombination frequency and distribution across eukaryotes: patterns and processes. *Philosophical Transactions of the Royal Society B: Biological Sciences* 372.
- Sztepanacz, J. L., and M. W. Blows, 2017 Artificial Selection to Increase the Phenotypic Variance in *gmax* Fails. *American Naturalist* 190: 707-723.
- Thornton, K. R., 2019 Polygenic Adaptation to an Environmental Shift: Temporal Dynamics of Variation Under Gaussian Stabilizing Selection and Additive Effects on a Single Trait. *Genetics* 213: 1513-1530.
- Turelli, M., 1984 Heritable Genetic-Variation Via Mutation Selection Balance - Lerch Zeta Meets the Abdominal Bristle. *Theoretical Population Biology* 25: 138-193.
- Turelli, M., and N. H. Barton, 2004 Polygenic variation maintained by balancing selection: pleiotropy, sex-dependent allelic effects and G x E interactions. *Genetics* 166: 1053-1079.
- van Kleunen, M., and M. Fischer, 2005 Constraints on the evolution of adaptive phenotypic plasticity in plants. *New Phytology* 166: 49-60.
- Walsh, B., and M. Lynch, 2018 *Evolution and selection of quantitative traits*. Oxford University Press, New York, NY.

- Walter, G. M., J. D. Aguirre, M. W. Blows and D. Ortiz-Barrientos, 2018 Evolution of Genetic Variance during Adaptive Radiation. *The American Naturalist* 191: E108-E128.
- White, H., 1980 A Heteroskedasticity-Consistent Covariance-Matrix Estimator and a Direct Test for Heteroskedasticity. *Econometrica* 48: 817-838.
- Wright, S., 1931 Evolution in Mendelian Populations. *Genetics* 16: 97-159.
- Wright, S., 1932 *The roles of mutation, inbreeding, crossbreeding, and selection in evolution*. na.
- Xu, L., H. Chen, X. Hu, R. Zhang, Z. Zhang *et al.*, 2006 Average gene length is highly conserved in prokaryotes and eukaryotes and diverges only between the two kingdoms. *Molecular Biology and Evolution* 23: 1107-1108.
- Zhang, X. S., 2012 Fisher's geometrical model of fitness landscape and variance in fitness within a changing environment. *Evolution* 66: 2350-2368.
- Zhang, X. S., and W. G. Hill, 2002 Joint effects of pleiotropic selection and stabilizing selection on the maintenance of quantitative genetic variation at mutation-selection balance. *Genetics* 162: 459-471.

Tables

Table 1: Model parameters for both null and stabilizing selection models. The range of values is based on literature, but values are adjusted to be practical for the time of the experiment.

Parameter	Symbol	Range	Description	Source(s)
Genome-wide recombination rate	r	0 to 1.241×10^{-4} per locus	The singular recombination rate used across the entire simulated genome.	(STAPLEY <i>et al.</i> 2017)
Background selection rate	δ_{μ}	0 to 1	The ratio of non-trait, deleterious mutations that occur relative to trait mutations.	
Rate of universal pleiotropy	ϖ	0 to 0.5	The proportion of trait mutations that affect all traits rather than a single trait. While 100 loci control a trait independently by default, this might be changed by this parameter. However, ratios of loci affecting each trait will remain constant, especially across multiple replicates.	(CHESMORE <i>et al.</i> 2018)
Mutational pleiotropic correlation	m	0 to 0.5	The mutational correlation between additive effects of pleiotropic mutations determines the similarity of trait effects between traits for the same pleiotropic mutation.	
Additive effect size	α	0.1 to 10	Additive effect size controls the variance of trait effect size around mean 0, so that $N(0, \alpha)$.	(ALBERT <i>et al.</i> 2008; LE CORRE AND KREMER 2012)

Selection strength (selection model only)	τ	10 to 10000	The parameter that controls the curve of the fitness function (eq. 3), with higher values resulting in a smaller difference in fitness between trait-differing individuals.
---	--------	-------------	---

Table 2: Means (\bar{x}), standard errors (S.E.) and counts (n) of distance from the phenotypic optimum (τ), variance (V_A), and covariance among traits for levels of additive effect size, recombination rate, pleiotropy rate, and mutational correlations for Gaussian and House-of-Cards models. Values in bold are mentioned in the main text and featured in Figures 5, 6, or 7. Values in italics indicate means that include outliers that were excluded from figures 6 and 7 for better readability. * denotes values of interest.

		δ			V_A			Covariance		
		Null	House-of-Cards	Gaussian	Null	House-of-Cards	Gaussian	Null	House-of-Cards	Gaussian
Additive effect size (α)										
Low	\bar{x}	11.151	0.715	1.384	1.035	0.241	1.747	0.069	0.002	0.015
	S.E.	0.133	0.033	0.065	0.067	0.013	0.025	0.008	0.0002	0.002
	n	545	458	445	545	458	445	545	458	445
Medium	\bar{x}	-*	3.109	2.085	-	9.733	3.120	-	-0.699	0.034
	S.E.	-	1.110	0.213	-	8.590	0.163	-	0.709	0.010
	n	0	6	26	0	6	26	0	6	26
High	\bar{x}	-*	1.202	2.699	-	110.240	2.943	-	-9.932	-0.022
	S.E.	-	0.258	-	-	57.536	-	-	5.077	-
	n	0	3	1	0	3	1	0	3	1
Recombination rate										
Low	\bar{x}	10.349	0.664	1.543	0.822	4.151	1.595	0.066	-0.452	0.006
	S.E.	0.197	0.066	0.101	0.063	3.080	0.026	0.013	0.371	0.003
	n	267	46	234	267	46	234	267	46	234
Medium	\bar{x}	11.452	1.372	1.467	0.898	5.941	3.412	0.068	-0.355	0.043
	S.E.	0.191	0.289	0.219	0.079	5.297	0.408	0.009	0.357	0.011
	n	219	37	2	219	37	2	219	37	2
High	\bar{x}	13.658	0.699	1.310	2.507*	0.232	2.048	0.089	0.002	0.024
	S.E.	0.241	0.033	0.076	0.418	0.012	0.048	0.022	0.0002	0.002
	n	59	37	236	59	384	236	59	384	236

		δ			V_A			Covariance		
		Null	House-of-Cards	Gaussian	Null	House-of-Cards	Gaussian	Null	House-of-Cards	Gaussian
Pleiotropy rate										
Low	\bar{x}	10.965	1.073	1.736	0.846	2.011	1.912	0.056	-0.194	0.003
	S.E.	0.137	0.127	0.100	0.037	1.559	0.046	0.007	0.196	0.002
	n	512	85	270	512	85	270	512	85	270
Medium	\bar{x}	14.139	1.024	0.966	4.472	3.458	1.786	0.465	-0.207	0.042
	S.E.	0.288	0.114	0.077	0.623	2.438	0.040	0.098	0.167	0.003
	n	15	83	109	15	83	109	15	83	109
High	\bar{x}	13.952	0.581	1.063	3.539	0.140	1.639	0.113	0.002	0.019
	S.E.	0.308	0.028	0.067	1.362	0.006	0.047	0.060	0.0002	0.003
	n	18	299	93	18	299	93	18	299	93
Mutational correlation										
Low	\bar{x}	13.722	0.629	1.499	1.559	0.414	1.981	0.005	-0.016	0.0003
	S.E.	0.161	0.039	0.076	0.098	0.208	0.051	0.009	0.017	0.002
	n	117	253	238	117	253	238	117	253	238
Medium	\bar{x}	13.885	2.521	1.118	3.378	22.616	1.681	0.196	-1.461	0.016
	S.E.	0.240	0.778	0.100	0.509	21.752	0.054	0.036	1.468	0.002
	n	51	9	83	51	9	83	51	9	83
High	\bar{x}	9.983*	0.820	1.479	0.555	0.934	1.672	0.072	-0.077	0.039
	S.E.	0.148	0.054	0.145	0.031	0.647	0.030	0.009	0.081	0.004
	n	377	205	151	377	205	151	377	205	151

Table 3: Means (\bar{x}), standard errors (S.E.) and counts (n) of distributional statistics among traits for levels of additive effect size, recombination rate, pleiotropy rate, and mutational correlations for Gaussian and House-of-Cards models. Statistics include distribution variance (σ), kurtosis (β_2), and the number of mutations contributing to the distribution (n_μ). * denotes values of interest.

		σ			β_2			n_μ		
		Null	House-of-Cards	Gaussian	Null	House-of-Cards	Gaussian	Null	House-of-Cards	Gaussian
Additive effect size (α)										
Low	\bar{x}	0.132	0.792	1.248	5.50	3.523	3.278	943.852	697.771*	2092.61*
	S.E.	0.028	0.072	0.0753	0.129	0.025	0.021	35.012	15.41	57.973
	n	108	227	179	108	227	179	108	227	179
Medium	\bar{x}	14.684	9.584*	7.029*	4.934	7.889	4.165	1729.017	318	1373.944
	S.E.	0.254	3.303	0.546	0.041	2.670	0.105	49.967	85	154.99
	n	59	2	18	59	2	18	59	2	18
High	\bar{x}	-	25.762*	15.116*	-	5.182	7.918	-	231	1004
	S.E.	-	10.450	-	-	0.90	-	-	81	-
	n	0	2	1	0	2	1	0	2	1
Recombination rate										
Low	\bar{x}	7.166	3.020*	1.584	5.188	3.830	3.284	1158.097	309.091	1568.851*
	S.E.	0.711	1.695	0.132	0.100	0.338	0.041	51.823	11.115	38.344
	n	114	22	94	114	22	94	114	22.000	94
Medium	\bar{x}	1.353	3.420	13.914	5.946	3.652	4.852	1468.578	425.737	891
	S.E.	0.505	0.774	-	0.114	0.180	-	57.060	12.631	-
	n	45	19	1	45	19	1.000	45.000	19.000	1.000
High	\bar{x}	0.360	0.626*	1.963	3.224	3.538	3.456	729.875	761.068	2446.107*
	S.E.	0.018	0.061	0.256	0.086	0.027	0.056	29.836	14.283	82.763
	n	8	190	103	8	190	103	8	190	103

		σ			β_2			n_μ		
		Null	House-of-Cards	Gaussian	Null	House-of-Cards	Gaussian	Null	House-of-Cards	Gaussian
Pleiotropy rate										
Low	\bar{x}	0.096	2.805	2.176	5.541	3.512	3.305	920.859	370.222	1325.511
	S.E.	0.010	0.792	0.261	0.128	0.063	0.036	31.635	11.189	20.798
	n	106	45	88	106	45	88	106	45	88
Medium	\bar{x}	14.684	1.766	1.061	4.934	3.604	3.454	1729.017	486.611	2747.204
	S.E.	0.254	0.391	0.220	0.041	0.216	0.039	49.967	15.116	100.847
	n	59	36	54	59	36	54	59	36	54
High	\bar{x}	2.082	0.404	2.074	3.146	3.587	3.432	2162.500	835.427	2416.393
	S.E.	0.060	0.103	0.306	0.002	0.033	0.107	23.500	11.810	61.652
	n	2	150	56	2	150	56	2	150	56
Mutational correlation										
Low	\bar{x}	0.271	0.846*	2.276*	3.129	3.693	3.375	512.909	716.677	1433.188*
	S.E.	0.007	0.173	0.249	0.101	0.067	0.058	11.177	22.149	43.292
	n	11	127	101	11	127	101	11	127	101
Medium	\bar{x}	7.539	4.550	1.859	4.402	4.477	3.278	1890.714	367.250	2263.761
	S.E.	1.586	0.870	0.307	0.276	0.307	0.061	249.018	64.617	87.980
	n	14	4	46	14	4	46	14	4	46
High	\bar{x}	5.438	1.248*	0.973*	5.554	3.388	3.488	1210.113	670.050	2969.157*
	S.E.	0.612	0.369	0.216	0.078	0.030	0.057	33.982	21.247	46.501
	n	142	100	51	142	100	51	142	100	51

Figure legends

Figure 1: Populations with differing degrees of adaptedness hovering around a phenotypic optimum. Three different populations are represented with black (X_1), blue (X_2) and red (X_3) lines. Dotted lines indicate trajectories towards the phenotypic optimum, whilst dashed lines represent the paths of populations hovering around the phenotypic optimum. The size of arrow heads indicates the adaptability of populations, with larger arrowheads representing more rapid movement towards a phenotypic optimum, at the cost of more erratic movement when hovering around that phenotypic optimum.

Figure 2: Flow diagram of differences between modelled populations. House-of-Cards and Gaussian models represent two sides of Continuum of Alleles models, with implicit expectations for adaptedness versus adaptability. Lines represent chromosomes with dots representing trait mutations (black) or deleterious non-trait mutations (red). The size of the dots indicates their phenotypic/fitness effect. Adapted from Walsh and Lynch (2018), Figure 28.1.

Figure 3: Mean additive variance (V_A ; panel A) and mean between-trait covariance (B) over 100,000 generations of stabilizing selection of different strengths (τ). 256 total models were sampled across the spectrum of selection strengths ($\tau = (10, 1000)$) with an additional 1024 models sampling the null space of parameters ($\tau = 0$).

Figure 4: Euclidean distances from the phenotypic optimum (δ) over models. (A): total distributions of all models. (B): distributions of adapted models with small distance to the optimum.

Figure 5: Euclidean distances from the phenotypic optimum ($\bar{\delta}$) among adapted populations with increasing additive effect size (α). Note that there was only one adapted Gaussian population with high additive effect size, and three House-of-Cards with high effect size. Bars indicate S.E.M.

Figure 6: Mean additive variance (V_A) among adapted populations with increasing additive effect size (α). Note that there was only one adapted Gaussian population with high additive effect size, and three House-of-Cards with high effect size. Several outliers were removed for improved readability. Bars indicate S.E.M.

Figure 7: Mean trait covariance among adapted populations with increasing additive effect size (α). Note that there was only one adapted Gaussian population with high additive effect size, and three House-of-Cards with high effect size. Several outliers were removed for improved readability. Bars indicate S.E.M.

Figure 8: Density estimates of mutational effect sizes for adapted populations at generation 100,000 under House-of-Cards and Gaussian models, with differing additive effect size distributions.

Figure 9: Population adherence to a two-trait (T1 and T2) phenotypic optimum over time. Xs indicate population positions in phenotype space, with the size of the X corresponding to the magnitude of mutational variance in the population. Blue Xs represent populations under House-of-Cards models of allelic effects, where mutation rates are low relative to selection strength. Red Xs represent populations under Gaussian models, where mutation rates are high relative to selection.

Supplementary Figures

Figure S1: Ratio of deleterious mutations to QTL mutations with increasing deleterious mutation rate. Note that odds of deleterious mutation to QTL go from 100% QTL at $x = 0$ to 50% QTL 50% deleterious at $x = 1$.

Figure S2: Preliminary analysis of mean heterozygosity over time with changing population size. Solid lines represent mean trajectories of 20 replicates, with ribbons representing standard errors. Dotted lines represent expected heterozygosities $\pm 5\%$, given by $\theta = 4N_e\mu$.

Figure S3: Latin hypercube sampling of null models (A) and selection models (B). Diagonals represent distributions of samples, which approximate uniformity. Points in bottom off-diagonal indicate a single sample in the parameter space. Each sample was replicated 100 times with unique seed values. Correlations in upper off-diagonal indicate maximum correlations between samples.

Figure S4: Interaction between additive effect size variability (α) and Continuum of Alleles model on the probability of reaching the phenotypic optimum ($P(o)$) by generation 100,000. Means measured over 128,000 observations. Error bars indicate S.E.M.

Figure 1

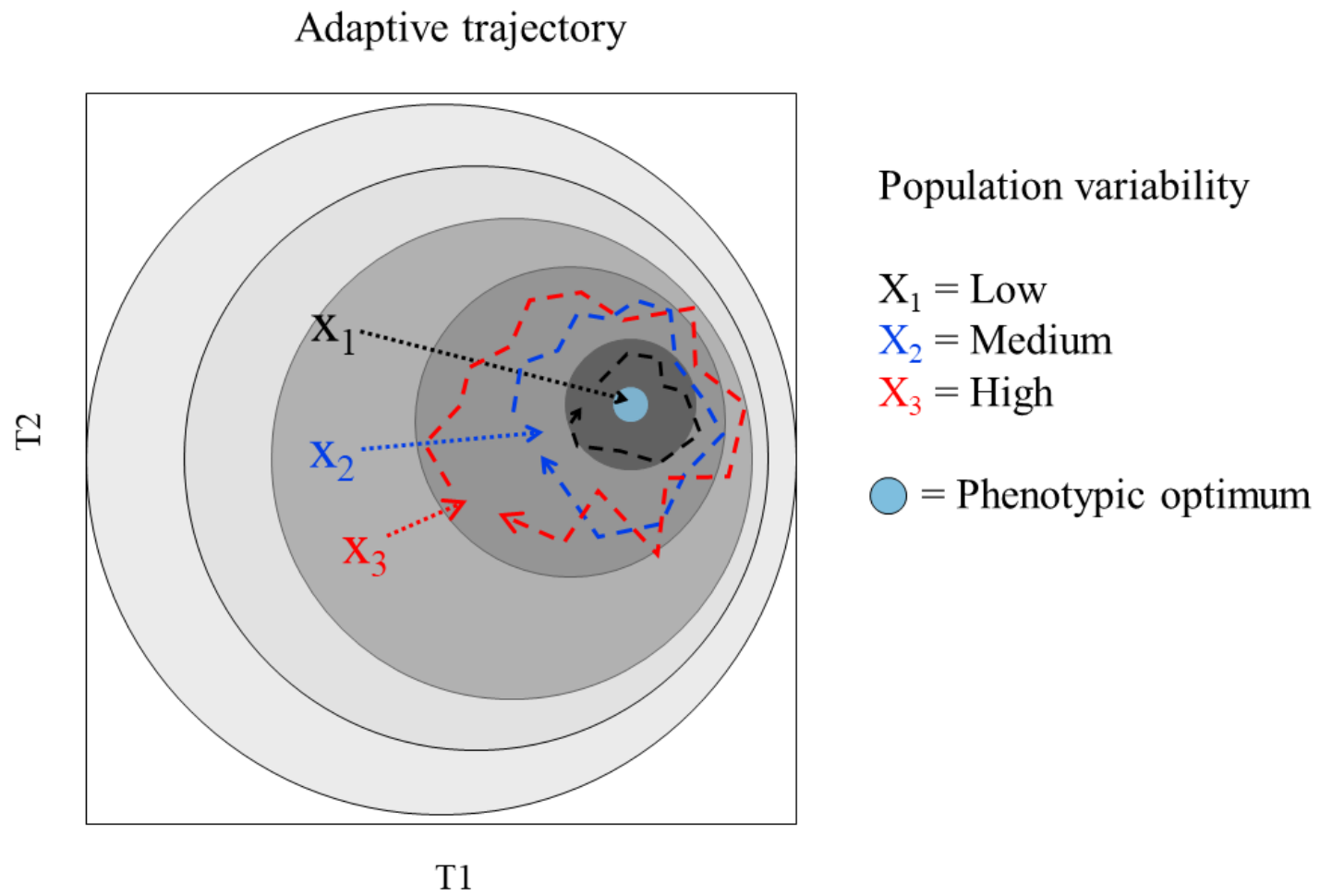


Figure 2

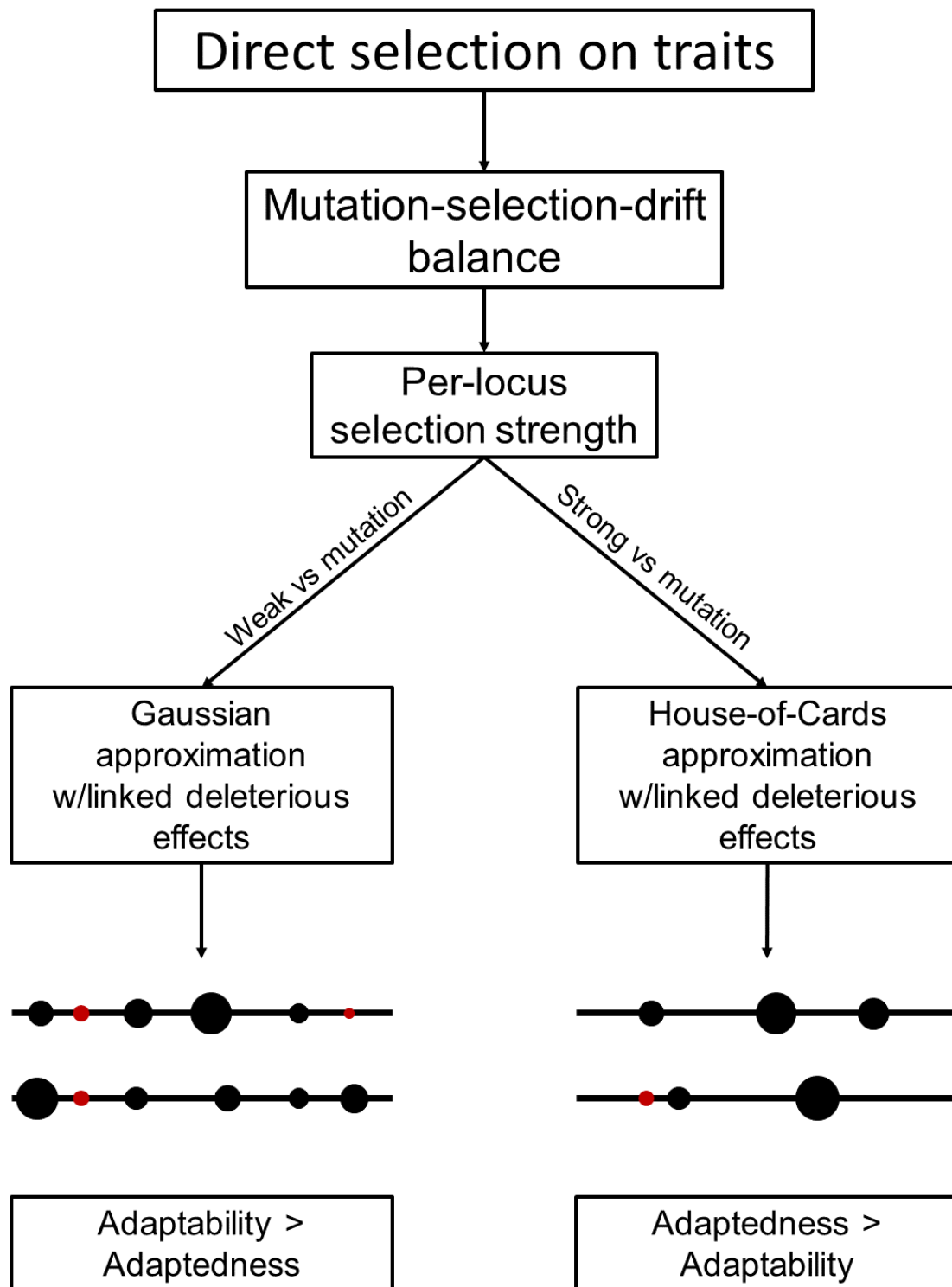
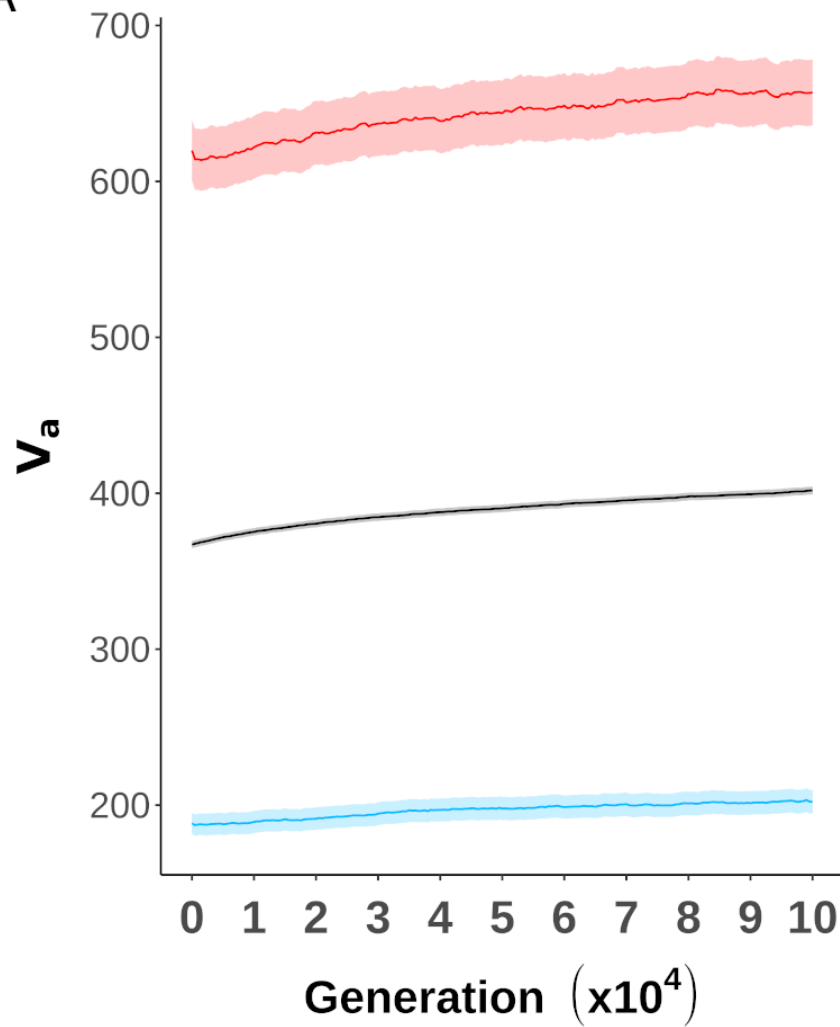
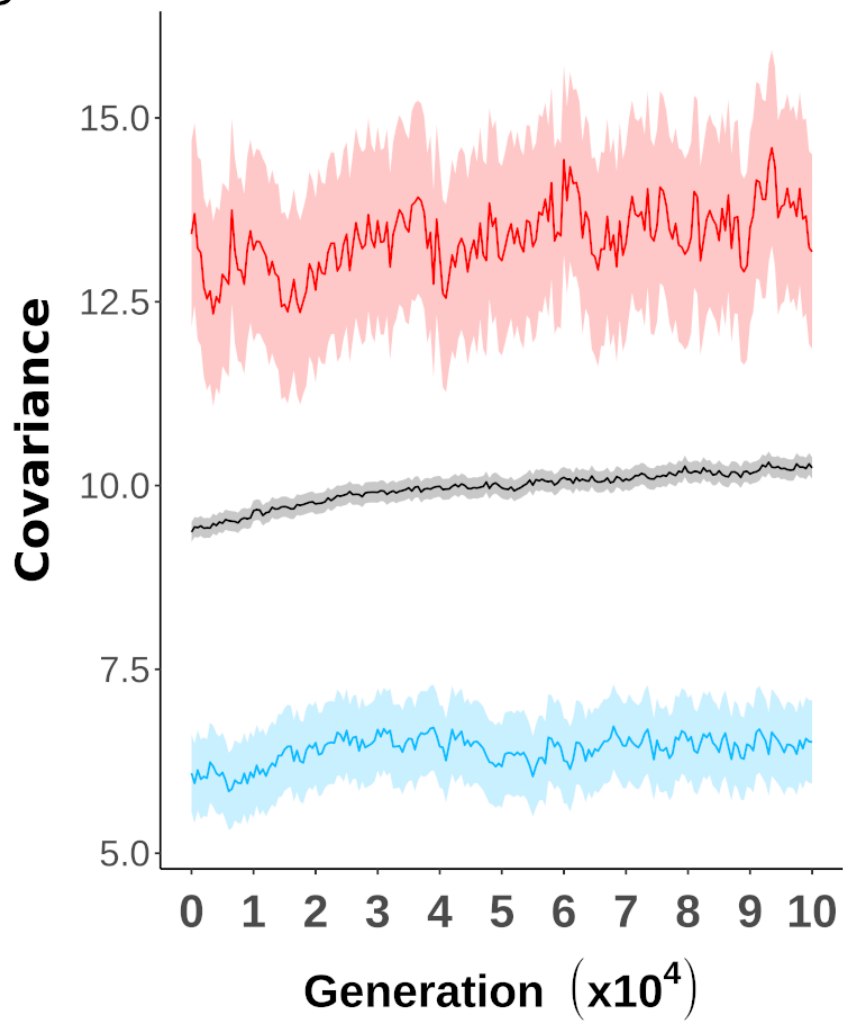


Figure 3

A



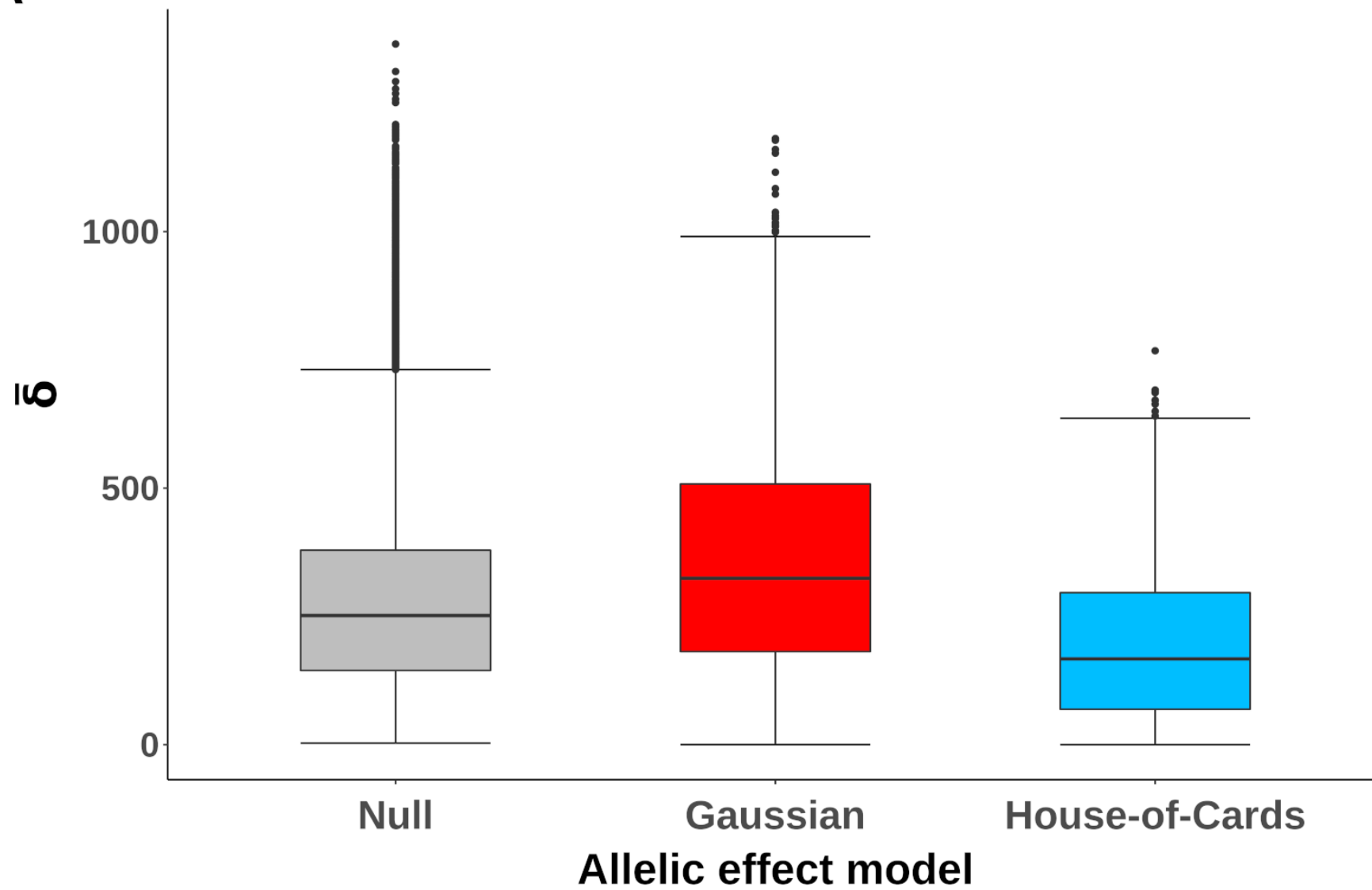
B



Allelic effect model: — Null — House-of-Cards — Gaussian

Figure 4

A



B

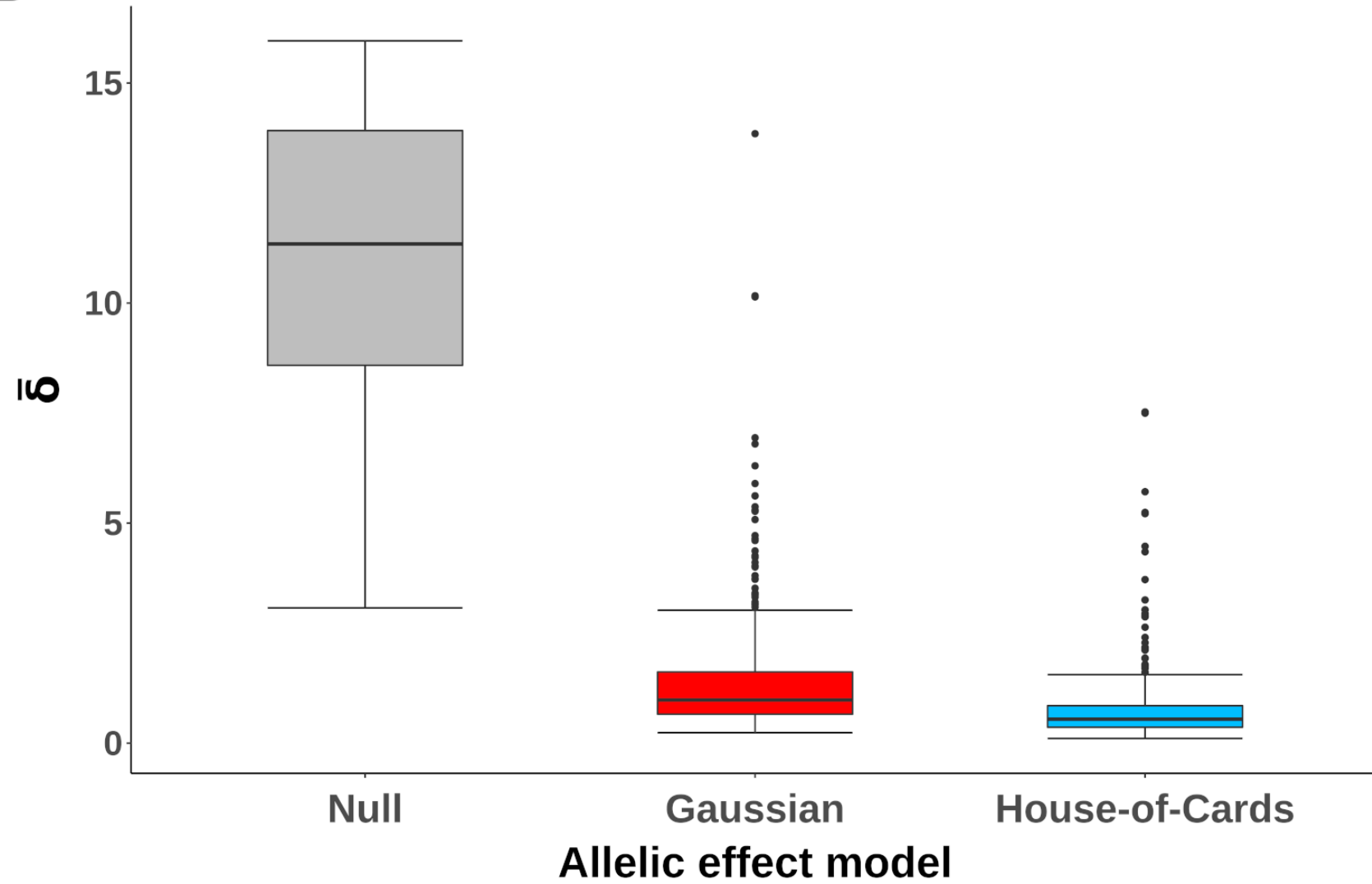


Figure 5

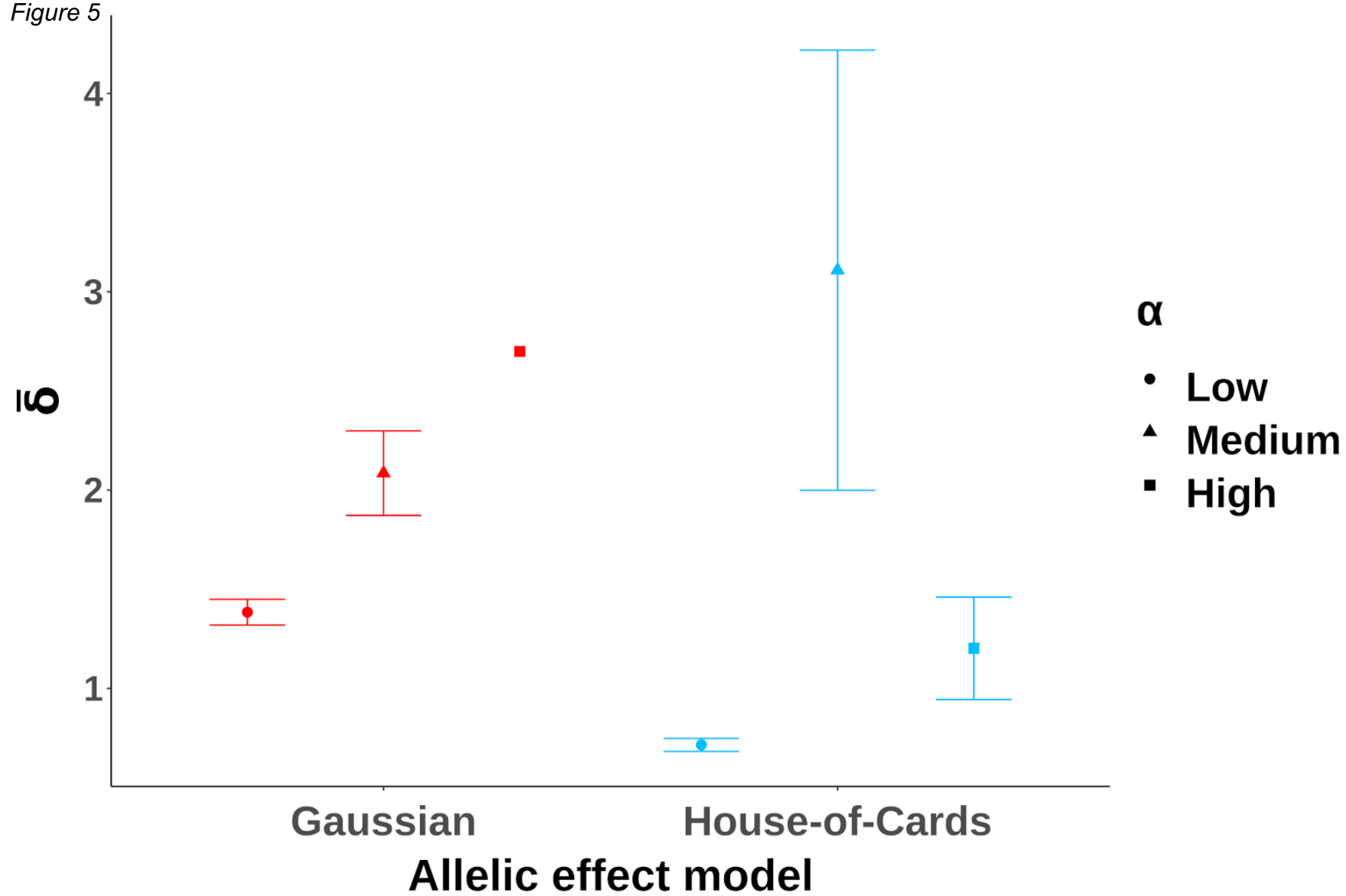


Figure 6

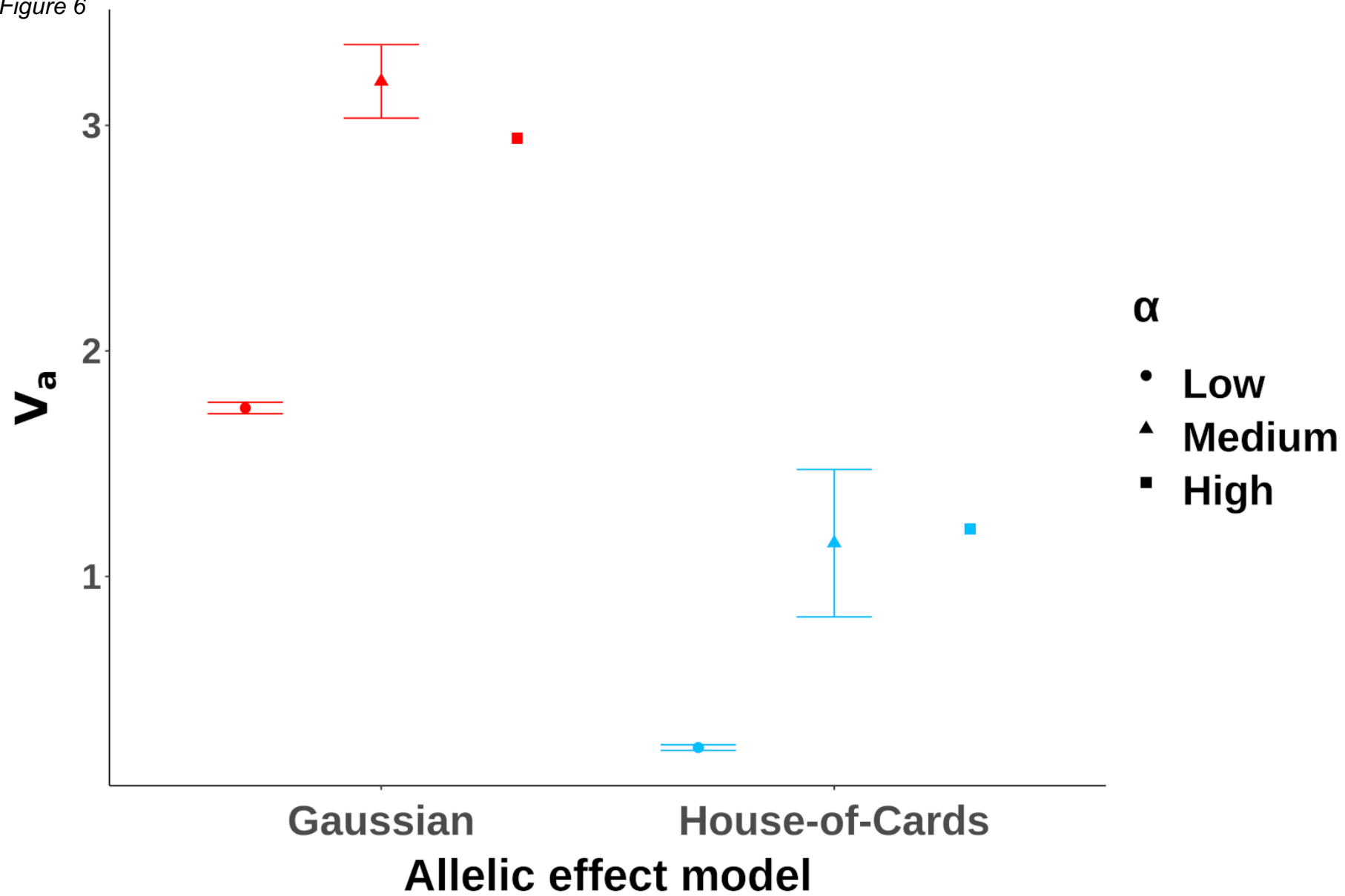


Figure 7

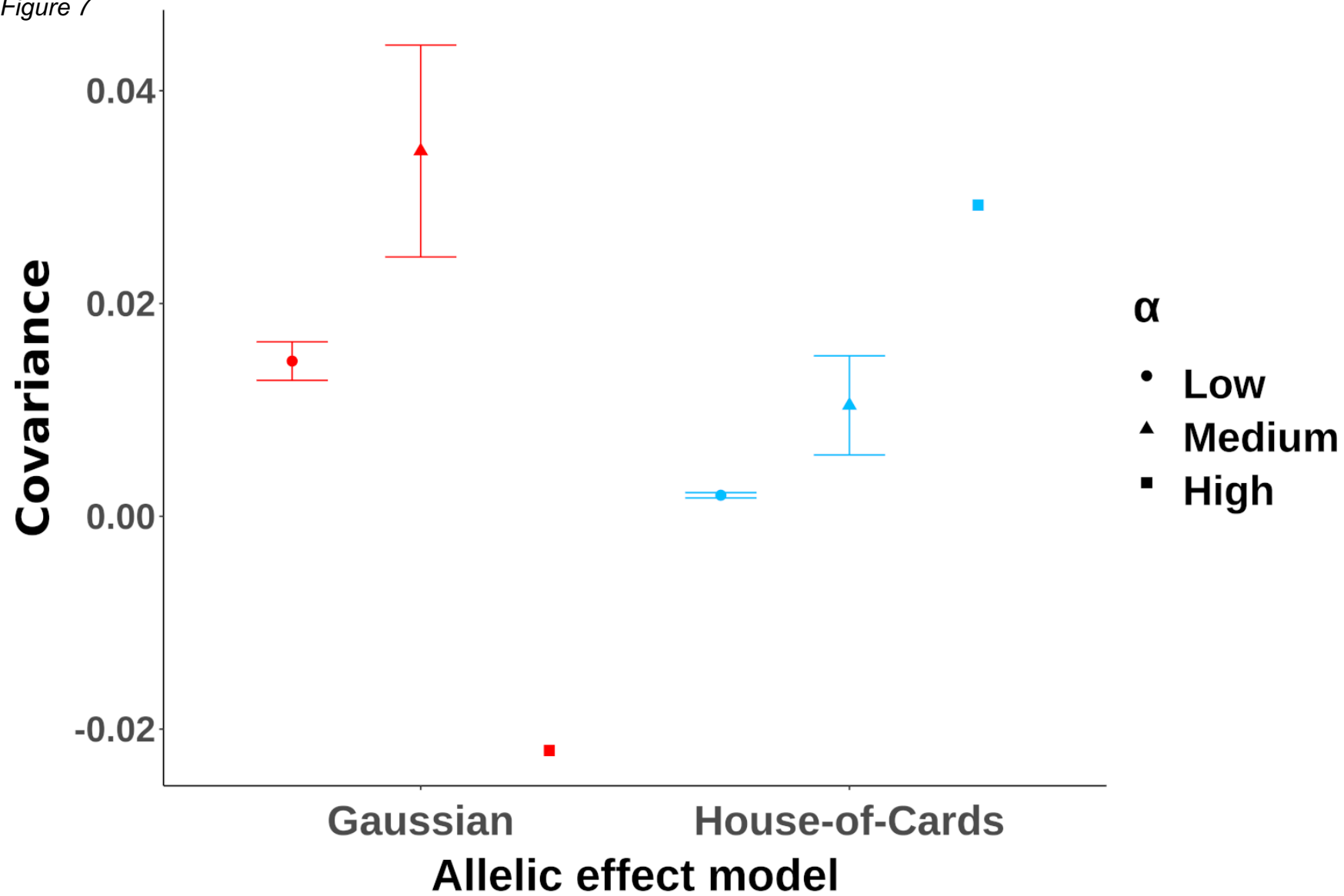


Figure 8

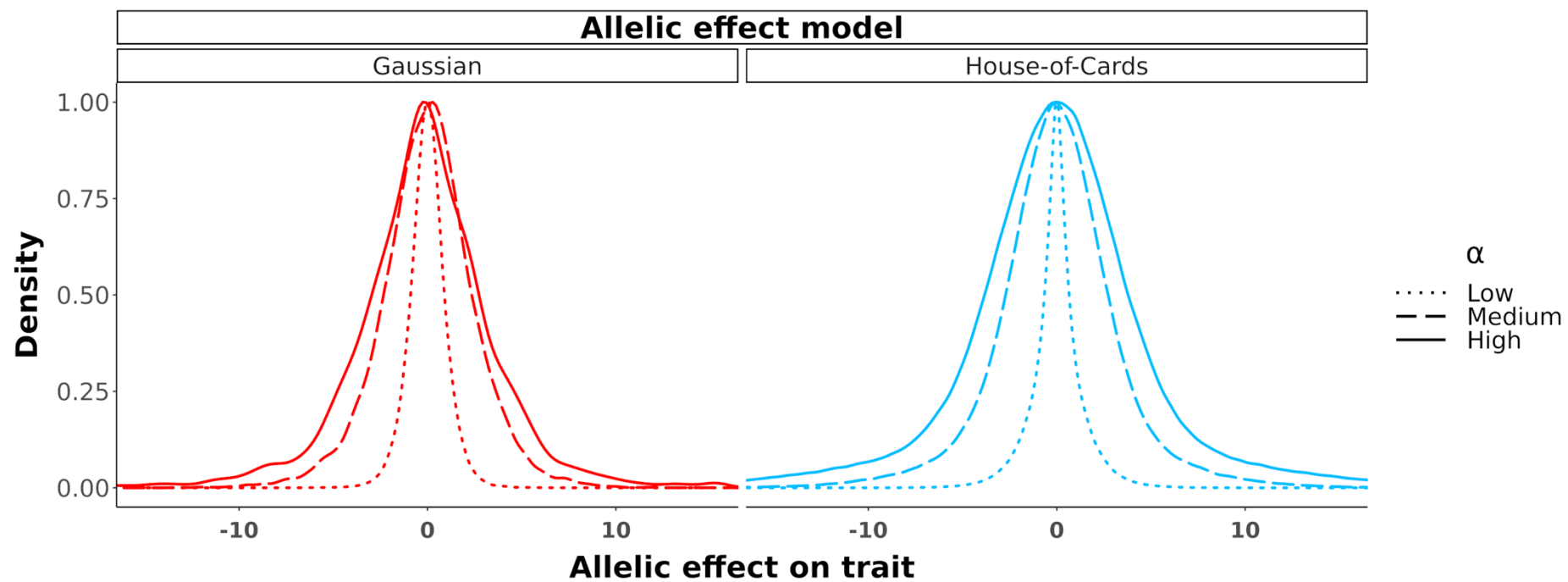
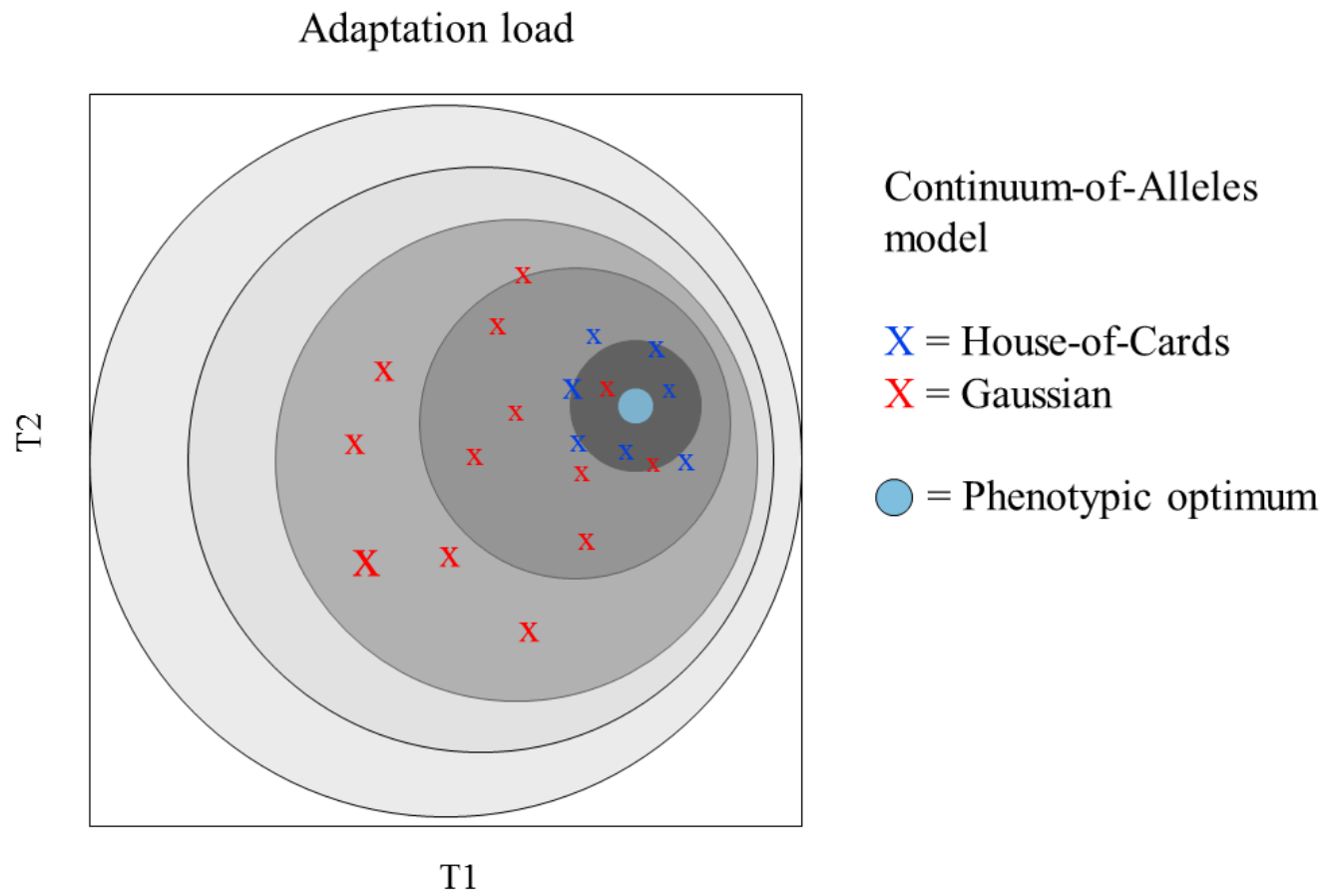


Figure 9



Supplementary figures

Figure S1

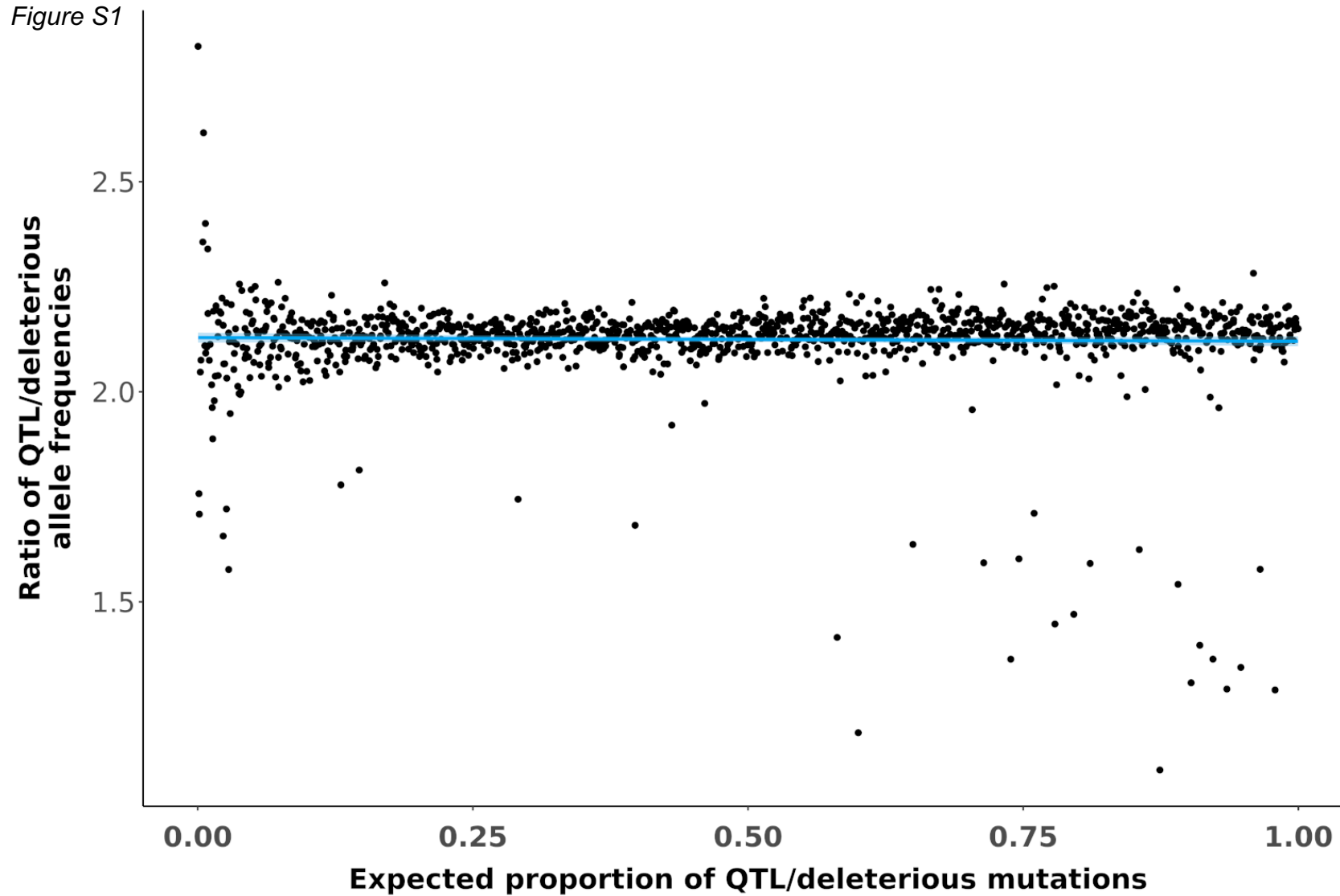


Figure S2

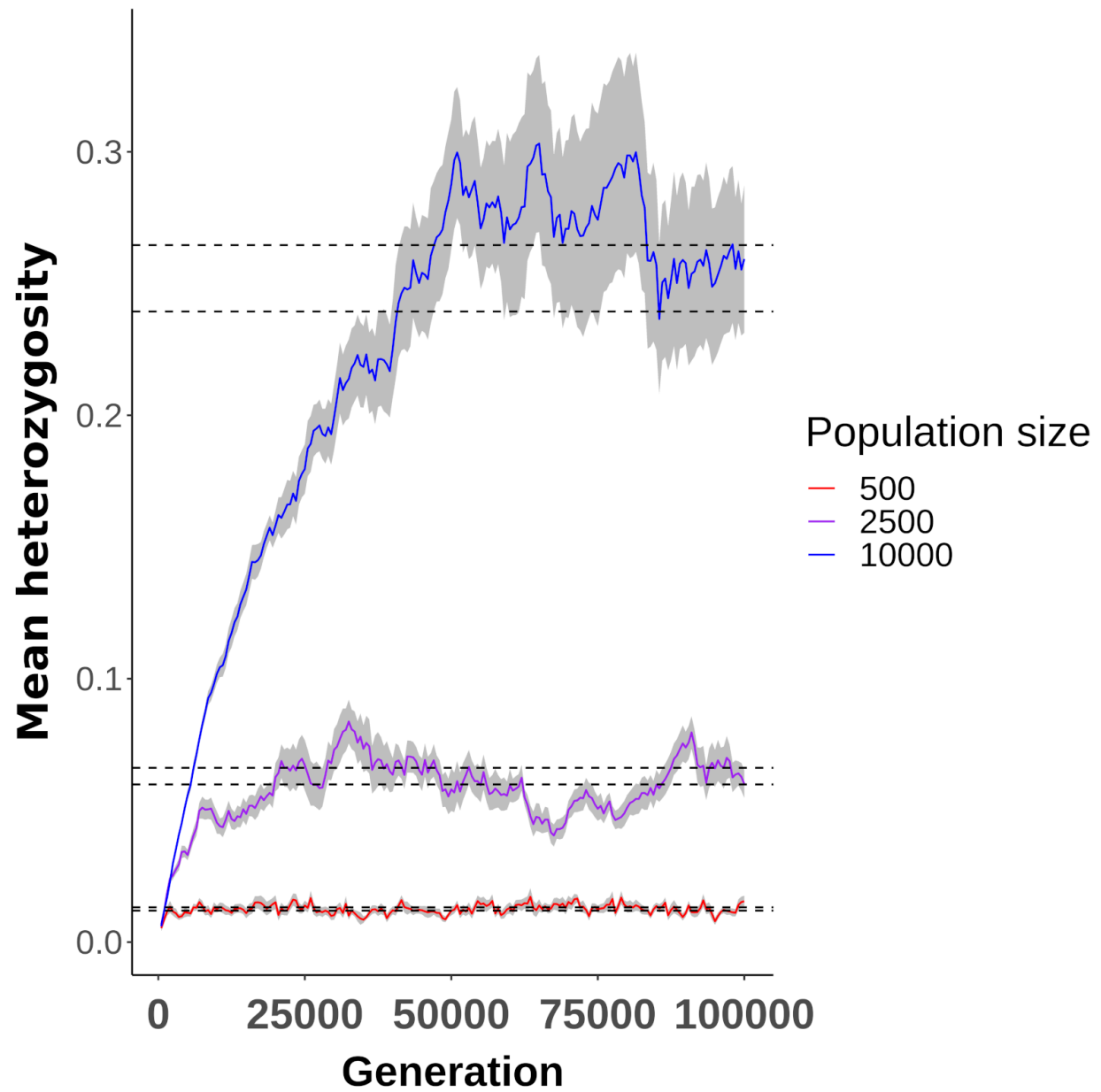
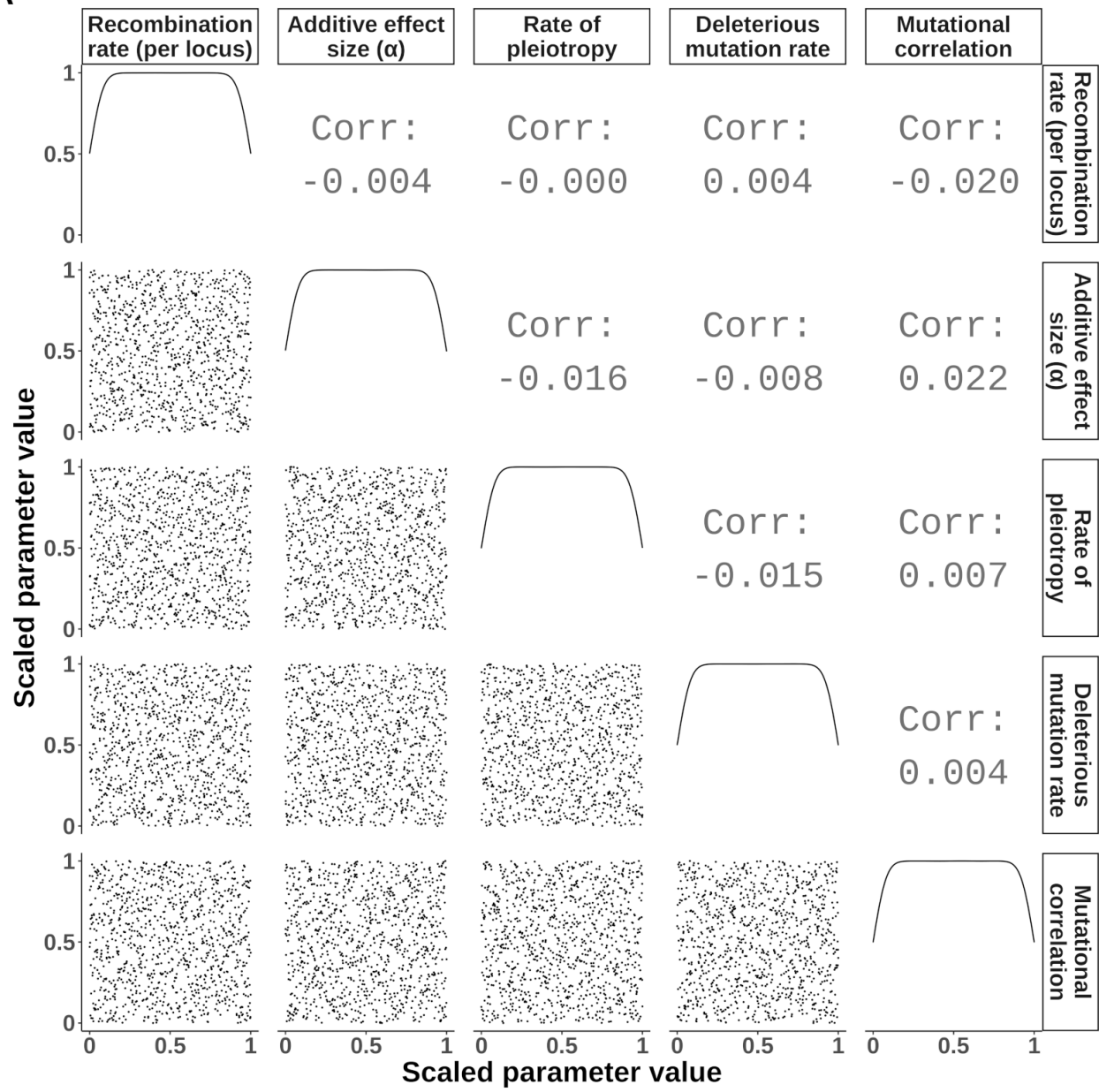


Figure S3

A



B

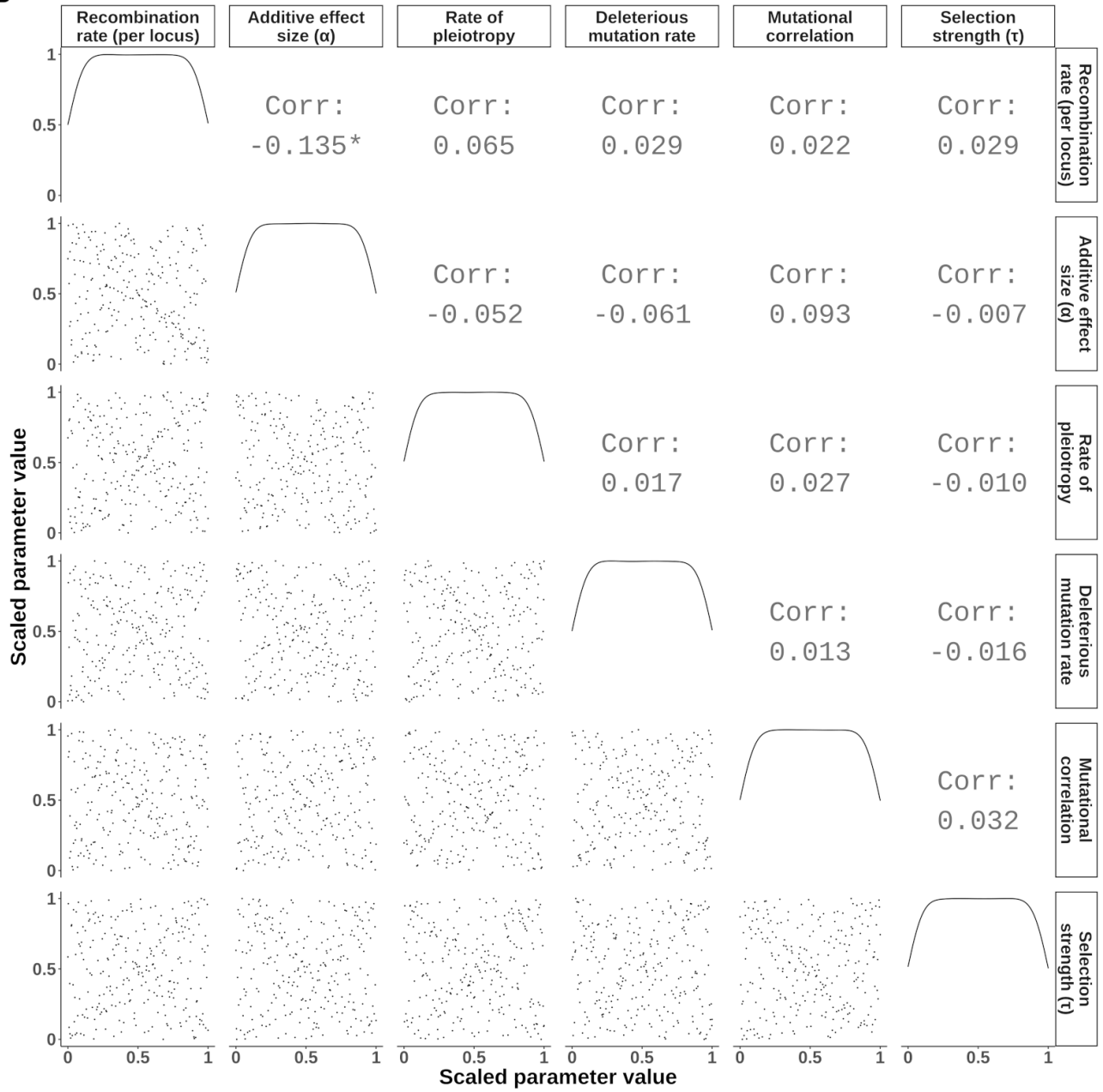
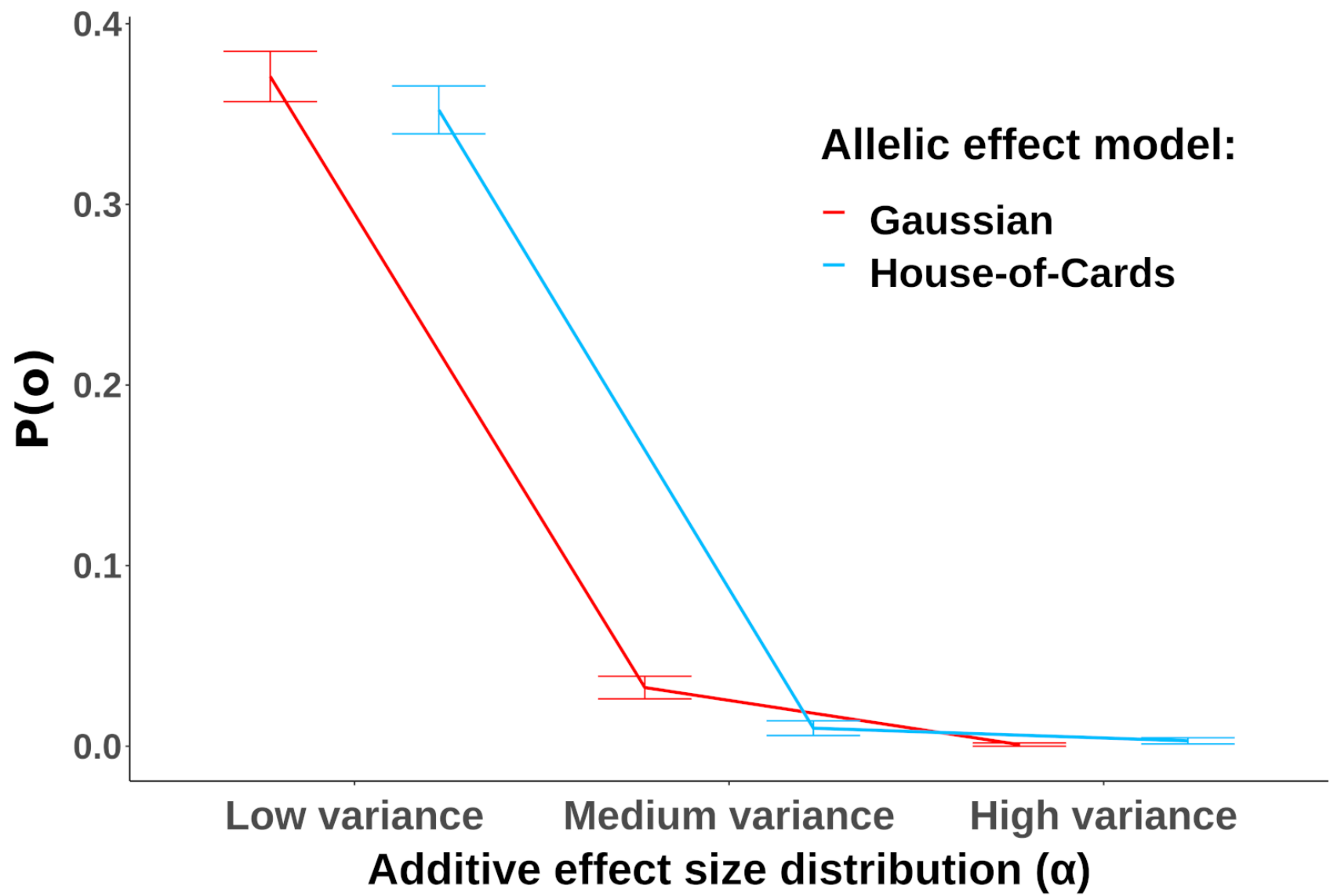


Figure S4



End of Document